



WAP-1D-VAR v1.0: Development and Evaluation of a One-Dimensional Variational Data Assimilation Model for the Marine Ecosystem Along the West Antarctic Peninsula

Hyewon Heather Kim^{1,2}, Ya-Wei Luo³, Hugh W. Ducklow⁴, Oscar M. Schofield⁵, Deborah K. Steinberg⁶, Scott C. Doney¹

5

¹Woods Hole Oceanographic Institution, Woods Hole, MA 02543, United States

²University of Virginia, Charlottesville, VA 22904, United States

³Xiamen University, Xiamen, Fujian 361102, China

⁴Lamont-Doherty Earth Observatory, Columbia University, Palisades, NY 10964, United States

10 ⁵Rutgers University, New Brunswick, NJ 80901, United States

⁶Virginia Institute of Marine Science, Gloucester Point, VA 23062, United States

Correspondence to: Hyewon Heather Kim (hkim@whoi.edu)

Abstract

15 The West Antarctic Peninsula (WAP) is a rapidly warming region, with substantial ecological and biogeochemical responses to climate change and variability for the past decades, revealed by multi-decadal observations from the Palmer Antarctica Long-Term Ecological Research (LTER) program. The wealth of these long-term observations provides an important resource for ecosystem modelling, but there has been a lack of focus on the development of numerical models that simulate time-evolving plankton dynamics over the Austral growth season along the coastal WAP. Here we developed a one-dimensional, data assimilation planktonic ecosystem model (i.e., the WAP-1D-VAR model v1.0) equipped with a variational adjoint and model parameter optimization scheme. We first demonstrate the modified and newly added model schemes to the pre-existing food-web and biogeochemical components of the WAP-1D-VAR model, including diagnostic sea-ice forcing and trophic interactions specific to the WAP region. We then conducted model experiments by assimilating eleven different data types from an example Palmer LTER growth season (October 2002 - March 2003) directly related to corresponding model state variables and intercompartmental flows. The iterative, data assimilation procedure reduced by 80% the misfits between observations and model results, compared to before optimization, via an optimized set of 14 parameters out of total 72 free parameters. The optimized model results captured key WAP ecological features, such as blooms during seasonal sea-ice retreat, the lack of macronutrient limitation, and comparable values of the assimilated and non-assimilated model state variables and flows to other studies, as well as several important ecosystem metrics. One exception was slightly underestimated particle export flux, for which we discuss fully potential underlying reasons. The data assimilation scheme of the WAP-1D-VAR model enabled the available observational data to constrain previously poorly understood processes, including the partitioning of primary production by different phytoplankton groups, the optimal chlorophyll to carbon ratio of the WAP phytoplankton community, and the partitioning of dissolved organic carbon pools with different lability. The WAP-1D-VAR model was successfully employed to glue the snapshots from a range of the available data sets together to explain and understand the observed dynamics along the coastal WAP.

20
25
30



35 1 Introduction

The West Antarctic Peninsula (WAP) has experienced significant atmospheric and surface ocean warming since the 1950s, resulting in decreased winter sea-ice duration, retreat of glaciers, and changes in upper ocean dynamics (Clarke et al., 2009; Cook et al., 2005; Henley et al., 2019; King, 1994; Meredith & King, 2005; Stammerjohn et al., 2008; D. Vaughan et al., 2003; D. G. Vaughan, 2006; Whitehouse et al., 2008). These climate-driven changes propagate through marine food-webs
40 by affecting physiology of individual organisms and the whole communities (Hugh W Ducklow et al., 2007). Long-term observational efforts through the Palmer Antarctica Long-Term Ecological Research program (LTER; since 1991) have demonstrated a range of ecological and biogeochemical responses to changing environments, including phytoplankton (Montes-Hugo et al., 2009; Saba et al., 2014; Schofield et al., 2017), marine heterotrophic bacteria (Bowman & Ducklow, 2015; Hugh W. Ducklow et al., 2012; Kim & Ducklow, 2016; Luria et al., 2014, 2017), nutrient drawdown (Kim et al., 2016),
45 and micro- and macrozooplankton (L. Garzio & Steinberg, 2013; Steinberg et al., 2015; Thibodeau et al., 2019).

The wealth of Palmer LTER time-series observations provides an important resource for ecological modelling, and different types of ecological modelling approaches have been developed to explore the WAP responses to climate change and variability. For example, an inverse modelling study estimated the steady-state dynamics of the WAP food-web by deriving snapshots of intercompartmental flows among different plankton functional types and higher trophic levels (Sailley et al.,
50 2013). However, there has been a less focus on numerical ecosystem models that simulate time-evolving plankton dynamics over the full Austral growth season along the WAP. Numerical ecosystem models provide estimates of key rate processes for which observations have been less frequently or seldom made compared to frequently measured stocks and rates. Despite its strength, constructing an ecosystem model is a challenge due to the lack of *a priori* knowledge on model parameters and incomplete understanding of ecological processes that should be explicitly presented in the model structure (H. W. Ducklow
55 et al., 2008; Murphy et al., 2012). Owing to many observational studies, a more robust, yet still incomplete, data-based picture is emerging of WAP food-web interactions and ecosystem dynamics, which could guide a development of the WAP-specific numerical ecosystem model.

Here we introduce a one-dimensional variational data assimilation model specific to the coastal WAP (i.e., the WAP-1D-VAR model v1.0) that we developed by adapting an existing biogeochemical-planktonic model of different ocean basins
60 (Friedrichs, 2001; Friedrichs et al., 2006, 2007; Luo et al., 2010). The WAP-1D-VAR model is compared against the roughly semi-weekly, bio-physical observations over the Austral growth season near Palmer Station on Anvers Island, Antarctica (64.77°S, 64.05°W). The field data record the seasonal variations in phytoplankton bloom initiation, peak and termination and biogeochemistry modulated by variations in surface light, mixed layer depth, and sea-ice cover. In the present study, we 1) describe the structure and schemes of the WAP-1D-VAR in great detail, 2) evaluate the model performance and robustness
65 using a variety of quantitative metrics, and 3) discuss the model applicability with regard to capturing the key WAP ecological and biogeochemical features using the data from an example growth season.

2 Model development and implementation

2.1 Model state variables

The WAP-1D-VAR model v1.0 (Figure 1) is originally derived and modified from data-assimilative, ocean regional
70 test-bed models of the Arabian Sea, the Equatorial Pacific, and the Hawaii Ocean Time-series Station ALOHA (Friedrichs, 2001; Friedrichs et al., 2006, 2007; Luo et al., 2010). The WAP-1D-VAR model simulates stocks and flows of C, N, and P through 12 different model prognostic state variables. The two size-fractionated phytoplankton compartments, diatoms and cryptophyte, and the two different zooplankton compartments, microzooplankton and krill are separately simulated following



75 the plankton functional types as in Saille et al (2013). Functional grazing relationships are defined in which diatoms are consumed by both krill (*Euphausia superba*) and microzooplankton (mostly ciliates and other protozoa), cryptophytes are consumed by microzooplankton, and microzooplankton are grazed by krill. Other abundant zooplankton taxa in the WAP (e.g., salps, pteropods, and copepods; Steinberg et al. 2015) are not explicitly simulated in the WAP-1D-VAR model, in part to limit the model complexity and in part because of limited data constraints on these groups, especially feeding. Higher trophic levels are implicitly represented to close the model. The WAP-1D-VAR model allows for the partitioning between labile DOM (LDOM) and semi-labile DOM (SDOM) such that the entire LDOM pool is available but only a limited portion of the SDOM is available for bacterial utilization to account for lower lability of SDOM. Refractory DOM (RDOM) is not explicitly modelled due to its much longer turnover time than labile and semi-labile pools, but some mass flows are included to RDOM from other prognostic model compartments, such as bacteria, krill, and SDOM, to account for loss terms for those state variables. Detritus represents an average particulate organic matter (POM) pool after removing living phytoplankton and bacterial biomasses, and sinking of the detritus pool contributes to export flux. The WAP-1D-VAR model explicitly simulates NO_3 , NH_4 , and PO_4 for inorganic (macro)nutrient compartments, but there is not a separate Fe model compartment or Fe uptake processes, given that iron limitation is absent or occurs only minimally and seasonally in the nearshore Palmer Station area (Sherrell et al., 2018).

2.2 Model equations

Here we describe key model processes that are either based on existing schemes or built as new, modified schemes for the WAP. The original model schemes are detailed in Supplementary Material of Luo et al (2010). The WAP-1D-VAR model simulates biological-physical model processes for a 1-D vertical water column, solving numerically for a discretized version of the time-rate of change for each model state variable. For a generic tracer variable C the time-rate of change equation takes the form (Glover et al., 2011):

$$\frac{\partial C}{\partial t} = -\frac{\partial}{\partial z}(wC) + \frac{\partial}{\partial z}\left(K_z \frac{\partial C}{\partial z}\right) + J_C \quad (1)$$

95 where z is the depth, w is the vertical velocity (the sum of water motion and gravitational particle sinking), K_z is the turbulent eddy diffusivity (Eq. 1), and J_C is the biological and biogeochemical net source and sink term for C (Appendix Equations Eq. A.2.41-44, A.3.37-40, A.4.53-55, A.5.24-26, A.6.27-29, A.7.4-6, A.8.4-9, A.9.2-4). The physical advection and mixing terms are discussed below in section 2.3 and are applied sequentially following the computation of the biological and biogeochemical terms J_C using a constant time step Δt of 1 hour. The contributions of the source sink terms J_C to the full time rate of change equations are constructed as a series of coupled ordinary differential equations, detailed in Appendix (sections A1-9), and are solved using a second-order Runge-Kutta numerical integration scheme. The WAP-1D-VAR model simulates the dynamics of C, N, and P, but here we only focus on the presentation of the model C dynamics. The cellular molar (N/C or P/C) quota parameters of most state variables are fixed and not submitted to the optimization and data assimilation procedure. To first order, a variety of the model physiological processes are affected by water temperature, including the maximum growth rates of phytoplankton, bacteria, and zooplankton and basal respiration rates of bacteria and zooplankton. The Arrhenius function is implemented to change these physiological rates as a function of water temperature (Eq. A.1.1).

110 The net change of phytoplankton (both diatoms and cryptophytes) C biomass is driven by their gross growth, DOC excretion, particulate organic C (POC) production via aggregation, respiration, and grazing (Eq. A.2.41, A.3.37), the net change of their N and P biomass by gross growth, dissolved organic N(P) (DON(P)) excretion, particulate organic N(P) (PON(P)) production, and grazing (Eq. A.2.42-43, A.3.38-39), and the net change of their chlorophyll a (Chl) by gross growth, DOM excretion, and grazing (Eq. A.2.44, A.3.40). The WAP-1D-VAR model adapts a phytoplankton growth scheme with flexible stoichiometry, in which phytoplankton cells are allowed to accumulate and store more nutrients under light stress (Bertilsson et al., 2003; Droop, 1974, 1983; McCarthy, 1980). The phytoplankton C growth rate is limited by their cellular nutrient contents (quota) (Eq. A.2.1-2, A.3.1-2). Modified from Geider et al. (1998), phytoplankton N uptake decreases when



115 their cellular N/C quota is higher than their reference (Redfield) ratio, but not limited when lower than their reference ratio
(Eq. A.2.4, A.2.8, A.3.4, A.3.8). The N consumption completely ceases when the phytoplankton cellular quota reaches their
maximum allowable ratios and additionally limited by the ambient nutrient concentrations with a Monod function (Eq. A.2.10-
11, A.3.10-11). NH_4 inhibition on NO_3 uptake is modelled by assigning lower k^{NH_4} compared to k^{NO_3} (Table 2). The inhibition
term does not exist for PO_4 . The uptake scheme is similar for P (Eq. A.2.13, A.3.13), but P can be consumed in great excess
120 of current needs (Armstrong 2006). Such luxury uptake is modelled by assigning smaller maximum and minimum P quota
(Table 2), which acts to alleviate P limitation. The maximum photosynthesis rate decreases when the phytoplankton cellular
quota is lower than their reference ratio, and approaches zero near their minimum ratio (Eq. A.2.6, A.3.6). The Chl production
decreases with lowering photosynthetic active radiation (PAR) and completely ceases under no light, i.e., $\text{PAR} = 0$ (Eq. A.2.14,
A.3.14). Phytoplankton release LDOM via passive diffusion of the low molecular weights DOM (e.g., neutral sugars and
125 dissolved free amino acids) with the same cellular elemental ratio as that of phytoplankton (Fogg 1966, Bjørnsen 1988,
Biddanda and Benner 1997) (Eq. A.2.16-18, A.3.16-18). Phytoplankton also release L- and SDOM actively, such as
carbohydrate, as 75% of the labile (Eq. A.2.19, A.2.23, A.3.19, A.3.23) and 25% of the semi-labile pools (Eq. A.2.20, A.2.26,
A.3.20, A.3.26). This active DOM production enables phytoplankton to adjust their stoichiometry to approach their reference
ratio. If cellular organic C is in excess, DOC is released on a time scale of 2 days, and if excess N(P), DON(P) is released on
130 a time scale of 8 days (Eq. A.2.21-22, A.3.21-22). Diatoms are grazed by both microzooplankton and krill (Eq. A.2.33-40),
while cryptophytes are only grazed by microzooplankton (Eq. A.3.33-36). Microzooplankton grazing functions are altered by
assigning grazing limitation terms (ϵ) to provide a limit on diatom grazing and route more cryptophytes to microzooplankton
(Eq. A.2.33, A.3.33), based on initial modelling attempts where elevated diatom Chl were not simulated due to their much
stronger removal by microzooplankton than cryptophytes, even with a varying model initial parameter set and adjusted baseline
135 parameters.

The net change of bacterial biomass is driven by their gross growth (via L- and SDOM uptake; Eq. A.4.12-14, A.4.15-
16, A.4.21-22), respiration (Eq. A.4.25), S- and RDOM excretion (Eq. A.4.26-28, A.4.35-43), grazing (Eq. A.4.44-46), and
mortality due to viral attack (Eq. A.4.47-49). The WAP-1D-VAR model allows both L- and SDOM as the sources for bacteria,
and bacterial nutrient quota let the lability of SDOM variable for their selective utilization. All the LDOM pool is available,
140 while only a limited portion of the SDOM pool is allowed for bacterial utilization, the degree of which is controlled by an
optimizable parameter controlling the relative utilization of SDOM to LDOM, or SDOM lability (Eq. A.4.11, Table 2).
Bacterial C growth is determined by their cellular quota and available L- and SDOM concentration (Eq. A.4.12-13), where the
growth would be limited if bacterial cellular N(P) quota is smaller than their reference ratios (Eq. A.4.8-9). Bacteria take up
LDOM in the way that the ratio of LDON(P) to LDOC uptake is the same as the bulk N(P)/C ratio of the LDOM (Eq. A.4.15,
145 Eq. A.4.21). Bacteria take up SDOM with higher N/P ratios to reflect that SDOM with higher N/P ratios is more labile (Eq.
A.4.13). The ratio of SDON to SDOC uptake by bacteria would vary between the bulk N/C of SDOM and the bacterial
reference cellular quota (Eq. A.4.16, Eq. A.4.22). Bacteria are modelled to either take up or release NH_4 and PO_4 to maintain
their rather stable and consistent stoichiometry (Kirchman, 2000). Bacteria take up NO_3 only if their cellular N/C ratio is
smaller than their reference ratio (i.e., when bacteria are in short of N), in order to reflect higher energetic cost of NO_3 uptake
150 than NH_4 , but the amount of NO_3 uptake is modelled to be no more than 10% of N-specific bulk L- and SDOM uptake, and
the NO_3 plus NH_4 uptake is modelled to be no more than N-specific bulk L- and SDOM uptake (Eq. A.4.17-20). These limit
the maximum NO_3 uptake rate and set the inhibition of NH_4 uptake on NO_3 uptake. Bacteria excrete RDOM by transforming
LDOM to RDOM (A.4.26-28). Bacteria adjust their cellular stoichiometry by remineralizing NH_4 and PO_4 if C in short (i.e., N
and P in excess; Eq. A.4.29-30) and by excreting SDOC if C is in excess (i.e., N and P are in short; Eq. A.4.38-43). Bacteria
155 are grazed by microzooplankton (Eq. A.4.44-46), and a certain percentage of bacteria gets lost to LDOC pool due to viral
attack (Eq. A.4.47-49).

The net change of zooplankton (both microzooplankton and krill) biomass is driven by their gross growth (via grazing
on preys; Eq. A.5.3-5, A.6.3-5), L- and SDOM excretion (Eq. A.5.6-14, A.6.6-14), respiration (Eq. A.5.17, A.6.17), POM



160 production (Eq. A.5.18-20, A.6.18-20), and grazing (Eq. A.5.21-23, A.6.24-26). Microzooplankton C growth is supported by
grazing on cryptophytes and bacteria (Eq. A.5.3-5), while krill C growth is supported by grazing on diatoms and
microzooplankton (Eq. A.6.3-5). Both zooplankton compartments follow the Holling Type 2 density-dependent grazing
function with a preferential selection on different prey species (Eq. A.2.33, A.2.37, A.3.33, A.4.44, A.5.21). Both zooplankton
groups release a portion of the organic matter that they ingest as DOM via sloppy feeding and excretion (Eq. A.5.6-8, A.5.9-
11, A.6.6-8, A.6.9-11) such that the ratio of the released DON(P) to LDOC is equivalent to the N(P)/C ratio of zooplankton.
165 The amount of SDOC excretion is a function of the total C growth (Eq. A.5.9, A.6.9), while the amount of SDON(P) excretion
is also a function of the zooplankton cellular N(P)/C ratio relative to their reference ratio (Eq. A.5.10-11, A.6.10-11).
Zooplankton adjust their body cellular quota by either releasing SDOM if C is in excess, or by regenerating NH₄ or PO₄ if N
or P is in excess (Eq. A.5.12-16, A.6.12-16), similar to the bacterial scheme. Respiration is formulated such that basal
respiration is based on a portion of zooplankton biomass, while active respiration is based on a portion of their grazed C (Eq.
170 A.5.17, A.6.17). Both zooplankton egest fecal matter as POM (Eq. A.5.18-20, A.6.18-20), but only krill additionally excrete
RDOM with N/C and P/C similar to bacteria (Eq. A.6.21-23). Microzooplankton are grazed by krill (Eq. A.5.21-23), while
krill are removed by implicit higher trophic levels (Eq. A.6.24-26), similarly calculated as a bacterial mortality term, rather
than as an explicit grazing process.

The net change of detritus is driven by POM produced by all phyto- and zooplankton compartments that is routed to
175 detrital pool (Eq. A.2.29-32, A.3.29-32, A.5.18-20, A.6.18-20) and its dissolution (Eq. A.7.1-3). An optimizable vertical
sinking speed is assigned to detritus to derive particle export fluxes (i.e., particle export flux = detrital concentration × particle
sinking velocity, w_{sv} in Table 2). The detritus that is lost due to dissolution is incorporated to SDOM pool when it sinks (Eq.
A.8.7-9), before regenerated to inorganic nutrients, rather than directly regenerated from as a particulate form. The net change
of LDOM is driven by LDOM excretion by all phyto- and zooplankton compartments (Eq. A.2.16-19, A.3.16-19, A.5.6-8,
180 A.6.6-8) and the amount of bacterial mortality that is incorporated to LDOM due to viral attack (Eq. A.4.47-49) and its uptake
by bacteria (Eq. A.4.12). The net change of SDOM is driven by SDOM excretion by all organisms (Eq. A.2.16-19, A.3.16-19,
A.5.6-8, A.6.6-8) and the amount of detrital dissolution (Eq. A.7.1-3), its uptake by bacteria (Eq. A.4.13-14), and its conversion
to RDOM pool (Eq. A.8.1-3). The conversion of SDOM to RDOM pool is a function of the stoichiometry of SDOM, in which
the conversion process is slower for higher N/C and P/C of the SDOM, to reflect that N- and P-enriched SDOM are more
185 likely labile. A certain percentage of NH₄ is converted to NO₃ on a daily basis to represent a simple nitrification process in the
model (Eq. A.9.1).

2.3 Physical forcing

The WAP-1D-VAR model v1.0 is forced by mixed layer depth (MLD), photosynthetically active radiation (PAR) at
the ocean surface, sea-ice concentration, water-column temperature, vertical velocity, and vertical eddy diffusivity, at a
190 temporal resolution of 1 day. Temperature, sea ice, and vertical eddy diffusivity are set up at every vertical grid (depth) point.

MLD is determined based on a finite difference density criterion with a threshold value of $\Delta\sigma_\theta = 0.03 \text{ kg m}^{-3}$ (Montégut
et al., 2004), after calculating potential density of water mass from temperature and salinity Conductivity-Temperature-Density
(CTD) observations. Vertical velocity, w , is assigned as zero because it is very weak in the surface waters of the study site (see
3.1), and materials are transported vertically mostly by diffusion. The vertical eddy diffusivity scheme treats the rapid vertical
195 mixing in the surface boundary layer by homogenizing model state variables instantaneously in the mixed layer by averaging
their values at every time step. Thus, K_z value above MLD is not required, and only K_z below MLD is calculated as follows:

$$K_z(z) = K_{z0} \times \exp\{-\alpha \times (z - MLD)\} \quad (2)$$

where z is depth (m) below MLD, K_{z0} is the vertical eddy diffusivity at the bottom of the mixed layer ($1.1 \times 10^{-4} \text{ m}^2 \text{ s}^{-1}$) (Klinck,
1998; D. A. Smith et al., 1999), and α is $0.01 \text{ (m}^{-1}\text{)}$.



200 Daily surface downward solar radiation flux (National Centers for Environmental Prediction reanalysis daily averages) is used to calculate sea surface PAR. PAR is estimated as 46% of the total solar radiation (Pinker & Laszlo 1992, Kirk 1994). The attenuation of PAR as a function of depth is calculated as follows:

$$PAR(z) = PAR_0 \times \exp\{-(k_w + k_c \times CHL) \times z\} \quad (3)$$

205 where z is depth (m), PAR_0 is PAR level at sea surface (W m^{-2}), k_w is the attenuation coefficient for seawater (m^{-1}), k_c is the attenuation coefficient for Chl ($(\text{mg Chl})^{-1} \text{m}^2$), and CHL is the Chl concentration (mg Chl m^{-3}).

210 Sea ice conditions in the coastal WAP do not necessarily represent solely local temperature and climate conditions, given that sea-ice concentration can be impacted by temperature, mixed layer, heat fluxes, regional winds, and other physical processes (Saenz et al. *in review*). We implement a sea-ice model scheme to account for light transmission through sea ice (5% of incident irradiance, a typical transmittance value used in the Community Earth System Model) and non-linearities in the photosynthesis-irradiance (P-I) response under partial ice concentration (Long et al. 2015), using percent daily sea-ice concentration data (GSFC Bootstrap versions 2/3, derived from SMMR/SSM/I satellite temperature brightness data binned into 25 by 25 km grid cells). In many previous models, the light-limitation term $\mathcal{L}(I)$ is calculated as a function of mean irradiance \bar{I} averaged over both ice-covered and open-water conditions, so $\mathcal{L}(\bar{I})$; instead we compute the mean of light-limitation term $\overline{\mathcal{L}(I)}$ as a function of fractional sea ice and open water and incident irradiance:

$$215 \quad \mathcal{L}(I) = P^C/P^C_{MAX} = 1 - \exp(-I/I_k) \quad (4)$$

$$\overline{\mathcal{L}(I)} = f_i \times \mathcal{L}(I_i) + f_o \times \mathcal{L}(I_o) \quad (5)$$

where P^C is the C-specific photosynthetic rate (d^{-1}), P^C_{MAX} is the maximum photosynthetic rate (d^{-1}), I_k is the parameter describing the light-saturation behaviour of the PI-curve (W m^{-2}), I_o is the open-water irradiance, I_i is the under-ice irradiance (i.e., $I_i = 0.05 \times I_o$), f_i is the fraction of area covered with sea ice, and f_o is the fraction of open water (i.e., $f_o = 1 - f_i$).

220 2.4 Variational data assimilation

The WAP-ID-VAR model v1.0 is equipped with a built-in data assimilation scheme based on a variational adjoint method (Lawson et al., 1995). By objectively optimizing model parameters, the assimilation method generates optimal solutions of the model that minimize model-observation misfit (Friedrichs, 2001; Spitz et al., 2001; Ward et al., 2010). Initial guesses of the model parameters (total of 72 free or optimizable parameters, Table 2) are assigned based on literature values, 225 or estimated directly using a subset of the observations. The data assimilation scheme (Figure 2) consists of four steps (Glover et al., 2011): 1) starting with an initial guess of the model parameter set, the model is integrated forward in time from specified initial conditions to calculate the difference between the model simulation and the field data, the model-observation misfit (i.e., cost function; see 2.5); 2) an adjoint model constructed using the Tangent linear and Adjoint Model Compiler (TAPENADE) is integrated backward in time to compute the gradients of the total cost with respect to the model parameters; 230 3) the computed gradients are then passed to a limited-memory quasi-Newton optimization software MIQN3 3.1 (Gilbert & Lemaréchal, 1989) to determine the direction and optimal step size by which the model parameters need to be modified in order to reduce the total cost; and 4) a new forward in time simulation is conducted using the new set of modified parameters. These procedures are conducted in an iterative manner until the pre-set convergence criteria are satisfied to ensure that the optimized parameters converge and the total cost reaches a local minimum. The pre-set convergence criteria include the low 235 gradients (sensitivity) of the total cost function with respect to model parameter from optimization and positive eigenvalues of the Hessian matrix. See Supplementary Material of Luo et al. (2010) for more details.

When computed at the minimum of the cost function value, the inverse of the Hessian matrix provides the uncertainties of optimized parameters, cross-correlations among parameters and sensitivities of the total cost to each parameter (Matear, 1996; Tziperman & Thacker, 1989). High off-diagonal values in the inversed Hessian matrix indicate highly cross-correlated model parameters, and one of the highly cross-correlated parameters is therefore removed from the optimization. 240 The square root of a diagonal element in the inversed Hessian matrix is the logarithm of the relative uncertainty of the



245 corresponding optimized parameter (i.e., σ_f). An optimized parameter with σ_f larger than 50% is updated but removed from the next optimization cycle, while the optimized parameter with σ_f smaller than 50% is updated and kept for the next optimization cycle. We define the optimized parameters with σ_f smaller than 50% as ‘optimized’ parameters and the optimized parameters with σ_f larger than 50% as ‘updated parameters’, with the former and the latter reported with and without their error ranges, respectively (Table 2). In other words, both changed parameters consist of an optimized model parameter set, but the parameters reported with their error ranges are the ones optimized with relatively small errors and therefore considered constrained. The absolute uncertainty of the constrained parameter is calculated as $p_f \times \exp(\pm\sigma_f)$ where p_f is the value of the optimized parameter. (Table 20).

250 2.5 Cost function

To represent a misfit between observations and model output, a total cost function is defined as follows (Luo et al., 2010):

$$J = \sum_{m=1}^M \frac{1}{N_m} \sum_{n=1}^{N_m} \left(\frac{\hat{a}_{m,n} - a_{m,n}}{\sigma_m} \right)^2 \quad (5)$$

255 where m and n represent assimilated data types and data points, respectively, M and N_m are the total number of assimilated data types and data points for data type m , respectively, σ_m is the target error for data type m , $a_{m,n}$ is observations, and $\hat{a}_{m,n}$ is model output. Given the high biological productivity of the WAP waters and the approximate log-normal distribution of many marine biological variables, the base-10 logarithms of Chl and primary production (PP) are used in the cost function calculation to capture phytoplankton dynamics (Campbell, 1995; Glover et al., 2018). The target error is calculated for each data type as:

$$\sigma_m = \overline{a_{m,n}} \times CV_m \quad (6)$$

260 where $\overline{a_{m,n}}$ is the climatological mean of the observations and CV_m is the coefficient of variation (CV) of the observations of each data type in the mixed layer (due to observational error and seasonal and interannual variations) over 2002-2003, 2003-2004, 2004-2005, 2005-2006, 2006-2007, 2008-2009, 2009-2010, 2010-2011, and 2011-2012 period (for growth seasons’ relatively complete data coverage for modelling purposes). The standard deviations are used as target errors of the log-converted data types. The CV of the log-converted data type is estimated as the average of ± 1 standard deviation in log space converted back into normal space (Doney et al., 2003; Glover et al., 2018). Hereafter, we present the total cost normalized by M (J equivalent to J/M hereafter) as it indicates the model-observation misfit equivalent to a reduced Chi-square estimate of model goodness of fit. We report the normalized total cost J along with normalized costs of individual data types (J_m) throughout this article. $J = 1$ indicates a good fit from optimization, $J \gg 1$ indicates a poor fit or underestimation of the error variance, and $J \ll 1$ indicates an overfitting of the data, fitting the noise, or overestimation of the error variance.

270 3 Model experiments

3.1 Modelling framework

275 To examine the applicability of the WAP-1D-VAR model v1.0 to the coastal WAP region, we selected a nearshore Palmer LTER water-column time-series station, Station E (64.77°S, 64.05°W), as the modelling site, that is situated approximately 3 km south of Palmer Station and 6.5 km northeast of the head of Palmer Deep (Sherrell et al., 2018). Physical forcing (Figure 3) and data types assimilated were derived from roughly semi-weekly physical, chemical and biological profiles collected from small boat via a profiling CTD and discrete water samples at Station E. When weather and ice conditions permitted, water column sampling at the station was conducted twice a week over the growth season since 1991. Seven upper-ocean layer depths (2.5, 10, 20, 30, 40, 50 and 60 m) were chosen for the model vertical grids. Given that routine observations



of Palmer LTER were conducted over the growth season (October - March), we simulated one example growth season with
280 the most complete data coverage, from October 2002 to March 2003 (2002-2003 growth season hereafter), instead of a series
of different growth seasons in a continuous manner. The example growth season simulations utilized that year's specific
observed physical forcing fields and assimilated biological and biogeochemical observations. In other words, each Palmer
LTER growth season would have its own unique optimized parameter set, as well as initial conditions and physical forcing
that together determine the model solution for that year; however, only 2002-2003 growth season simulations are modelled in
285 the present study for model analysis and evaluation.

3.2 Initial and boundary conditions

Model initial conditions were prescribed 135 days before the model start date for the growth season (October 15,
2002), so on June 1, 2002. This 135-day spin up was conducted to minimize the impact of initial conditions on the model
output over the growth season. Initial conditions were prepared by first generating an optimized model simulation of the full
290 growth seasonal cycle forced by climatological physics and assimilated with climatological observations (i.e., climatological
model; using climatological physics and observations averaged over 2002-2003, 2003-2004, 2004-2005, 2005-2006, 2006-
2007, 2008-2009, 2009-2010, 2010-2011, and 2011-2012 period). Due to strong interannual variability in the phytoplankton
bloom phenology at Palmer Station, averaging across all these 9 years did not reflect distinct seasonal phytoplankton peaks,
leading to underestimated phytoplankton values (not shown). To capture this non-linear aspect of the coastal WAP system, we
295 constructed the climatological year by applying a single time shift to all variables so that a seasonal PP peak of each year lined
up with an average date of seasonal PP peaks from all years. Most biological initial conditions on June 1 were close to zero
given the lack of active physiological processes in the very low light and the presence of sea ice during wintertime before the
model growth season started. All the data types were set to zero at the lower boundary (bottom) except for NO_3 , PO_4 , SDOC,
SDON, and SDOP in which the climatological values at 65 m were used for lower boundary values (25.9 mmol m^{-3} , 1.9 mmol
300 m^{-3} , 6.5 mmol m^{-3} , 0.6 mmol m^{-3} , and 0.03 mmol m^{-3} , respectively).

3.3 Assimilated data

We included data types directly related to corresponding model outputs, including a mix of ecosystem stocks or state
variables – NO_3 , PO_4 , Chl for diatoms and cryptophytes, bacterial biomass, microzooplankton biomass, SDOC, POC, and PON
as well as C flows among model stocks – bulk net PP and bacterial production (BP). The data were sampled semi-weekly at
305 Palmer Station E (64.77°S , 64.05°W), the same location where our model was set up, and were downloaded from the Palmer
LTER data website (see Availability of Data and Model Simulations). The distinction between diatoms and cryptophytes was
established by assimilating phytoplankton taxonomic-specific Chl data for diatoms and non-diatom species derived from a
High-Performance Liquid Chromatography (HPLC) and CHEMTAX analysis (Schofield et al., 2017), but given cryptophytes
being the second dominant species in the water samples they are considered to represent non-diatom species. Given that
310 POC(N) from bottle filtration might capture both living biomass and detrital material, we adjusted the observed POC(N) by
subtracting phytoplankton and bacterial C(N) biomass to estimate the detrital pool, in order to only include non-living particles
to detrital pool. When phytoplankton or bacterial biomass data were not available, we assigned climatological (2002-2003 to
2011-2012) fractions of POC(N) to detrital pool. Phytoplankton- and bacterial biomass accounted for 74% of total POC and
71% of total PON. In converting Chl to phytoplankton C(N) biomass, the maximum Chl/C(N) ratio submitted for optimization
315 was used along with other reference ratios (Table 2). Microzooplankton biomass data were not available for the full time-
series, so microzooplankton biomass data from grazing experiments at Palmer Station (L. M. Garzio et al., 2013) were
assimilated to at least provide constraints on bacterial and cryptophyte grazing processes. However, due to the discrepancy in
the timing and location from model simulations of this study, the microzooplankton model-observation misfits were not



320 examined in the present study. Krill biomass data were not assimilated due to the strong patchiness of their distribution that
might hinder proper model optimization. The vertical profiles of most of the data types were assimilated, whereas average NO_3
and PO_4 concentrations in the mixed layer were assimilated due to the difficulty of simulating depth-dependent nutrient
concentrations and the fact that net PP was mostly determined by surface nutrient concentrations (Luo et al., 2010). BP (mmol
325 $\text{C m}^{-3} \text{d}^{-1}$) was derived from the ^3H -leucine incorporation rate ($\text{pmol l}^{-1} \text{h}^{-1}$) data using the conversion factor of 1.5 kg C (mol
 leucine)^{-1} incorporated (H. W. Ducklow, 2000). Bacterial biomass (mmol C m^{-3}) was estimated from bacterial abundance
measured by flow cytometry with the conversion factor of 10 fgC cell^{-1} (Fukuda et al., 1998). SDOC was calculated by
330 subtracting the background concentration (41.2 mmol m^{-3} for the modelling site) from total DOC concentration.

3.4 Uncertainty analysis

Uncertainties of the optimized parameters were computed from a finite difference approximation of the complete
Hessian matrix (i.e., second derivatives of the cost function with respect to the model parameters) during the iterative
330 optimization process. We then conducted Monte Carlo experiments to calculate the impact of the optimized parameter
uncertainties on the model results. We created an ensemble of parameter sets ($N = 1,000$) by randomly sampling values within
the uncertainty ranges of the constrained parameters, and then performed a model simulation using each parameter set. 1,000
Monte Carlo experiments were shown to be adequate from a series of tests with different numbers of Monte Carlo sampling
($N = 500\text{-}2,000$), where standard deviations of model simulated values converged after $>1,000$ Monte Carlo sampling (not
335 shown). All uncertainty estimates were calculated following standard error propagation rules and presented as ± 1 standard
deviation in the article.

4 Results and discussion

4.1 Model skill assessment

In the case of the example growth season modelled in the present study (2002-2003 growth season), the iterative data
340 assimilation-parameter optimization procedure reduced by 80% the misfits between observations and model output compared
to the misfits with the initial guess parameters (Table 1). The optimized model solution also satisfied the pre-set convergence
criteria, with the low gradients of the total cost with respect to the optimized parameters and positive eigenvalues of the Hessian
matrix. Overall, there was a good model-data fit with largely decreased cost for each data type after optimization (Table 1).
There were three data types (NO_3 , diatom Chl, and bacterial biomass) that indicated a good fit from optimization, with their J_f
345 near 1, while none of the data types indicated a poor fit, or underestimation of the error variance. The average error or bias
(\mathcal{E}_{bias}) was calculated to evaluate the model over- or underestimation of the observations (Doney et al., 2009; Stow et al., 2009).
 \mathcal{E}_{bias} indicated negative biases (i.e., model underestimation of the observations) for NO_3 , diatom Chl, cryptophyte Chl, bacterial
biomass, SDOC, POC, and PON, while positive biases (i.e., model overestimation of the observations) for PO_4 , PP, and BP
(Table 1). Some of these model biases cases were evidently shown on a point-to-point basis, especially for POC and PON
350 (Figure B1). Model skill was further evaluated with a Taylor diagram (Taylor, 2001) summarizing the statistics of the
correlation coefficient, normalized standard deviation (by the standard deviation of the observations), and centred (bias
removed) root-mean-square difference (RMSD) for each data type (Figure 4). There were five data types with relatively high
correlation coefficients ($r > 0.5$) and five data types with relatively low correlation coefficients ($r < 0.5$). The data types with
relatively high correlation coefficients tended to have relatively low centred RMSD and vice versa. Together, the model fitted
355 average observations slightly better than the seasonal- and spatial (vertical) variability, given that the changes in the phase and



relative amplitude of the modelled variables relative to observations were not always strongly similar, despite small absolute model-observation differences for most data types.

4.2 Optimized parameters

Among the total of 72 optimizable model parameters, subsets of 14 (5 optimized and 9 updated) parameters changed compared to their initial guess values (Table 2). The number of the optimized parameters in the present study was small and comparable to the results from optimization of other regional test-bed models (Friedrichs, 2001; Friedrichs et al., 2006, 2007; Luo et al., 2010). This is consistent with the general behaviour of marine plankton ecosystem models, in which well-posed model solutions would be found with only a subset of independent model parameters due to many cross-correlated parameters inherent in nonlinear model equations (Fennel et al., 2001; Harmon & Challenor, 1997; Matear, 1996; Prunet, Minster, Echevin, et al., 1996; Prunet, Minster, Ruiz-Pino, et al., 1996). Ecosystem models with a relatively large number of unconstrained parameters (i.e., optimized parameters with high uncertainties, or updated parameters in the present study) might reduce total costs to a greater extent, but could possess low predictive skill as a result of being over-tuned to fit noise in the observations (Friedrichs et al., 2007).

The optimized model results at each model time step and grid were associated with generally small errors derived from the Monte Carlo experiments (Figure B2). To examine the translation of optimized parameters to altered functioning of the WAP biogeochemical processes, we compared two different sets of the model simulation results – one based on the initial guess parameters (i.e., before optimization; Figure B3) and the other based on the optimized parameters (i.e., after optimization; Figure 5, Figure B2). However, due to the non-linearities in the model it was not straightforward to identify what caused the parameter variations, except for a few cases in which the changes in the parameter values were clearly linked to the difference in the model results. One case was the relation of optimized θ (maximum Chl/N ratio, g Chl *a* (mol N)⁻¹) value to phytoplankton accumulations slightly more dominated by diatoms. The variations of θ are fundamentally driven by an imbalance between the rate of light absorption and energy demands for photosynthesis and biosynthesis in phytoplankton cells (R. J. Geider et al., 1997). θ can also change because of variations in phytoplankton photo-acclimation or physiological differences across phytoplankton groups, from a lower θ value for smaller species to a higher θ value for larger diatom cells (Richard J. Geider, 1987). In our case, θ was optimized to a value that is 10% higher than its initial guess value (Table 2), in order to simulate a relatively larger (smaller) proportion of diatoms (cryptophytes) in total phytoplankton biomass. μ_{KR} (maximum krill C-specific growth rate, d⁻¹) was optimized to about 2 times larger value than its initial guess value (Table 2), which resulted in larger krill accumulations in the optimized model results (Figure 5), compared to the unoptimized model results (Figure B3). By contrast, the remaining cases of the other parameters is less clear because the first-order impact of parameter variations on model results is less direct and more nuanced. Compared to the unoptimized results (Figure B3), d_{ISS} (detrital dissolution rate, d⁻¹) was optimized to 5 times smaller value relative to its initial guess value (Table 2), but overall there was decreased detrital accumulation in the optimized results (Figure 5) due to increased POC production by cryptophytes, microzooplankton, and krill in the optimized results (not shown). Similarly, compared to the unoptimized results, increased α_{DA} (initial slope of P-I curve of diatoms, mol C (g Chl)⁻¹ d⁻¹ (W m⁻²)⁻¹), g_{DA} (diatom half-saturation concentration in microzooplankton grazing, mmol C m⁻³), and g'_{DA} (diatom half-saturation concentration in krill grazing, mmol C m⁻³) did not necessarily lead to increased diatom accumulations, due to increased μ_{MZ} (microzooplankton C-specific maximum growth rate, d⁻¹) and μ_{KR} (maximum krill C-specific growth rate, d⁻¹). The three other cases were similarly interpreted: 1) The decreased α_{CR} (initial slope of P-I curve of cryptophytes mol C (g Chl)⁻¹ d⁻¹ (W m⁻²)⁻¹) and increased μ_{MZ} (microzooplankton C-specific maximum growth rate, d⁻¹), despite increased g_{CR} (cryptophytes half-saturation concentration in microzooplankton grazing, mmol C m⁻³), generated smaller cryptophyte accumulations in the optimized results; 2) the increased $r^A_{MAX,BAC}$ (bacterial maximum active respiration rate, d⁻¹) and μ_{MZ} (microzooplankton C-specific maximum growth rate, d⁻¹), despite increased μ_{BAC} (maximum bacterial growth rate, d⁻¹) and g_{BAC} (bacterial half-saturation



concentration in microzooplankton grazing, mmol C m^{-3}), generated smaller bacterial accumulations in the optimized results; and 3) the increased μ_{MZ} (microzooplankton C-specific maximum growth rate, d^{-1}) and g_{MZ} (microzooplankton half-saturation concentration in krill grazing, mmol C m^{-3}), despite increased μ_{KR} (maximum krill C-specific growth rate, d^{-1}) and $r^{4,MZ}$ (microzooplankton active respiration rate, d^{-1}), generated larger microzooplankton accumulations in the optimized results.

4.3 Ecosystem indices

We examined key ecosystem indices for the modelled year, including NPP (directly comparable to ^{14}C -PP observations), net community production (NCP; i.e., $\text{NCP} = \text{NPP} - \text{bacterial-}, \text{microzooplankton-}, \text{and krill respiration}$), BP integrated over the 60-m water column, and POC export (sinking) flux at 60-m (Figure 6, Figure B5). NPP increased after complete sea-ice retreat, but a brief ice-edge bloom was simulated under sea ice at the beginning of the growth season (Figures 3, 6). Seasonal patterns of NCP resembled those of NPP and occasionally fell below zero (Figure 6), indicating the net heterotrophy in subsurface waters. The depth-integrated NCP time series was moderately correlated to that of NPP over the growth season ($r = 0.78, p < 0.001$). The POC export flux increased over time and reached the maximum values at the end of the growth season (Figure 6). The depth-integrated POC export flux was also moderately correlated to that of NCP, with the POC export flux lagged by 15 days ($r = 0.51, p < 0.001$). The depth-integrated BP showed a similar seasonal pattern with and strongly correlated to that of NPP (Figure 6), with BP lagged by 2 days ($r = 0.94, p < 0.001$). The growth-season mean of the depth-integrated NPP, NCP, BP, and POC export flux at 60 m were $62 \pm 17 \text{ mmol C m}^{-2} \text{ d}^{-1}$, $17.3 \pm 19.6 \text{ mmol C m}^{-2} \text{ d}^{-1}$, $1.7 \pm 0.45 \text{ mmol C m}^{-2} \text{ d}^{-1}$, and $4.7 \pm 4.6 \text{ mmol C m}^{-2} \text{ d}^{-1}$ (errors propagated from season-averaging in Figure 6 and Monte Carlo errors in Figure B5). The mean e -ratio, defined as the growth-season mean of the time-lagged (by 15 days) POC export flux divided by the annual mean NPP (i.e., particle export efficiency), was 0.08 ± 0.06 . The mean f -ratio, defined as the amount of NO_3 uptake divided by the amount of NO_3 and NH_4 uptake both, was 0.66 ± 0.18 (errors propagated from season-averaging in Figure 7 and Monte Carlo errors in Figure B5). The mean BP/NPP ratio (also with time lagged BP by 2 days) was 0.03 ± 0.002 (errors propagated from season-averaging in Figure 6 and Monte Carlo errors in Figure B5).

Setting an upper limit for lateral or vertical carbon export from the euphotic zone (Dugdale & Goering, 1967), over appropriate time and space scales, NCP is quantitatively equivalent to new production that is supported via external sources of nitrogen (Hugh W. Ducklow & Doney, 2013). The higher mean f -ratio relative to the mean e -ratio in the present study implied an imbalance between production and export at the study site, at least during the modelled period. Excess new production relative to export production (as derived from sediment traps and ^{234}Th disequilibrium; see Ducklow et al. 2018) was previously observed in the WAP, presumably due to diel vertical migration, DOM export, lateral export, and diffusive loss of PON via diapycnal mixing (Stukel et al., 2015). Stukel et al (2015) reported up to 5 times larger new production via NO_3 uptake than export production via Th-based N export along the coastal WAP. There would be several additional mechanisms driving the discrepancy between production and export. First, given that the assimilated pool of suspended POC in the model formulation would not be a good indicator of a rapidly sinking detrital pool dominating particle export, our WAP-1D-VAR model did not capture large, short-lived particle flux events (e.g., fecal pellets produced by a large swarm of krill), underestimating POC export flux. Second, the WAP-1D-VAR model export scheme did not consider DOC export that would have lowered the production-export discrepancy. Finally, it should be noted that RDOC was not explicitly modelled in the WAP-1D-VAR, due to its much longer time scale than the model time scale, so accumulated and not-exportable RDOC pool would have contributed to derivation of the modelled e -ratio from the modelled f -ratio. Indeed, the modelled mean e -ratio in the present study situated at the lower end of the range of the e -ratios measured or estimated in the WAP waters (Hugh W. Ducklow et al., 2018; Saille et al., 2013; Stukel et al., 2015; Weston et al., 2013). By contrast, the modelled mean BP/NPP ratio corresponded well to the estimates from other measurement- and observation-based studies (Hugh W. Ducklow et al., 2012; Kim & Ducklow, 2016). Relatively low bacterial activity in productive Antarctic waters, typically reflected as a low



440 BP/PP ratio, has been attributed to low LDOM availability for bacterial growth (Kirchman et al., 2009), low temperature (Pomeroy & Wiebe, 2001), or top-down control via grazing and viral lysis (Bird & Karl, 1999).

4.4 Average C stocks and flows

We summarized the growth-season means of the C stocks and flows in the entire food web (Figure 7). The WAP-1D-VAR model captured several key WAP ecological and biogeochemical features, including the lack of macronutrient limitation (NO₃ and PO₄ drawdown by phytoplankton utilization but remaining well above their half-saturation constants, Table 2) and comparable values of the assimilated and non-assimilated model state variables (Hugh W Ducklow et al., 2007; Hugh W. Ducklow et al., 2012, 2018; Kim et al., 2016; Moline et al., 2008; R. C. Smith et al., 2008), providing confidence in the model simulations even for a non-assimilated data type such as krill. For instance, growth-season measurements in 2017-2018 at Palmer Station showed a strongly patchy krill distribution, with the mean biomass of 0.12 ± 0.04 mmol C m⁻³ and maximum biomass of 0.57 mmol C m⁻³ when krill were present (unpublished data provided by J. Conroy and D. Steinberg), falling in the range of the modelled krill biomass values (0.13 ± 0.06 mmol C m⁻³; calculated from Figure 7). The WAP-1D-VAR model also simulated several important ecosystem metrics comparable to other statistical modelling studies. For instance, the modelled phytoplankton seasonal patterns in the present study were consistent with physicochemical attributes revealed by a distinct ecological seascape pattern in the coastal WAP (Bowman et al., 2018), including low Chl and high nutrients in the first half of the growth season followed by high Chl and low nutrients in the second half of the growth season. A steady-state solution based, inverse modelling study quantified different food-web states using ecosystem network indices from Palmer LTER annual summer cruises along the WAP shelf region (Sailley et al., 2013). Their network indices included the ratio of C export to total PP (i.e., equivalent to *e*-ratio in the present study) and the ratio of recycling (the sum of flows into respiration and DOC pool) to total PP, where more (less) recycling favourable microbial food-webs were characterized by greater (smaller) ratios of recycling to total PP and smaller (greater) ratios of total C export to total PP (Legendre & Rassoulzadegan, 1996). As discussed above, the modelled mean *e*-ratio in the present study was smaller than the estimates in the inverse modelling study for the WAP shelf region (Sailley et al., 2013), but consistent with their conclusion on the food-web status of the modelled growth season (2002-2003) positioned on the microbial food-web side. The discrepancy in the *e*-ratio values between the present study and Sailley et al. (2013) might be attributed to fundamentally different model formulation (i.e., time-evolving modelling versus steady-state modelling) and optimization approach, or due to relatively strong microbial food-web activity at our coastal site compared to the shelf region. Microbial food-web activity can be approximated by quantifying the amount of fixed C flowing through heterotrophic bacteria (Carlson et al., 1999; del Giorgio & Cole, 1998; H. W. Ducklow, 2000; Hugh W. Ducklow et al., 2012). According to this approach, microbial food-web activity from the optimized model results was around $26 \pm 9\%$, calculated as the ratio of bacterial L- and SDOC uptake to PP (mean \pm error from season-averaging and Monte Carlo errors in Figure 7). SDOC appeared to be an important bacterial C source when LDOC became scarce as the growth season progressed (Figure 5), and on average, supported $19 \pm 7\%$ of the total bacterial C uptake, or C demand (mean \pm error from season-averaging and Monte Carlo errors in Figure 7). Indeed, several observational studies speculated that the WAP bacteria utilize SDOM in short of LDOM (Hugh W. Ducklow et al., 2011; Kim & Ducklow, 2016; Luria et al., 2017).

5 Summary

475 We developed the WAP-1D-VAR v1.0 model, a one-dimensional variational data assimilation model specific to the coastal WAP region, evaluated the model performance and robustness using a variety of quantitative metrics, and discussed the model applicability with regard to capturing the key WAP ecological and biogeochemical features using the data from an example growth season, 2002-2003. The data assimilation scheme significantly reduced the model-observation misfits via the



480 optimized model parameter set that adjusted the simulation to better match the Palmer LTER observations in 2002-2003. We
also explored the nuanced question of how the observations influenced the data assimilation process, drove the variations in
optimized parameter values relative to their corresponding initial guess values, and affected the resulting model simulations.
The WAP-1D-VAR model successfully simulated the variables and flows that were not assimilated in the model simulations,
with the values consistent with other measurement- and observation-based studies in the WAP. Importantly, the data
485 assimilation scheme enabled the available observational data to constrain processes that were poorly understood, such as the
partitioning of NPP by different phytoplankton groups, the optimal Chl/C ratio of the WAP phytoplankton community, and
the partitioning of DOC pools with different lability. Up to this point, a range of observational studies has provided snapshots
of ecosystem and biogeochemical processes in the WAP. Yet, we have little understanding of the driving processes that
underlie the connections between each component in complex food-web interactions. We used data-assimilative modelling to
490 glue these snapshots together to explain better the observed dynamics and further understand the previously poorly constrained
processes in the coastal WAP system.

Acknowledgements

We thank the many Palmer LTER team members and Palmer Station support staff for collecting, measuring, and
analyzing the field samples and for providing the datasets used in the present study. We also thank Le Xie for providing
495 protocols for the parameter optimization and adjoint models, Cristina Schultz for providing the initial guess values of the
model parameters, Nicole Waite for compiling HPLC data, and Joe Cope and Lori Garzio for compiling the zooplankton data.
Computing resources for model simulations were provided on the Rivanna high-performance computing system by the
Advanced Research Computing Services of the University of Virginia. Kim and Doney were supported by the National
Aeronautics and Space Administration Ocean Biology and Biogeochemistry Program (grant NNX14AL86G) and US National
500 Science Foundation Office of Polar Programs (grant PLR-1440435 to Hugh Ducklow at Columbia University; Palmer LTER).
Schofield and Steinberg were supported by US NSF grant PLR-1440435. Kim was also supported by the Investment in Science
Fund and the Reuben F. and Elizabeth B. Richards Endowed Fund from Woods Hole Oceanographic Institution. Luo was
supported by National Natural Science Foundation of China project 41890802.

505 Data availability

Complete Palmer LTER time-series data used for data assimilation are available online (<http://pal.lternet.edu/data>).
Surface downward solar radiation flux data used for physical forcing of the model simulations are found in the National Centers
for Environmental Prediction website (<https://www.esrl.noaa.gov/psd/data/gridded/data.ncep.reanalysis.surface.html>).

510 Code availability

The Tangent linear and Adjoint Model Compiler (TAPENADE) used to construct an adjoint model is available online
(<http://www.sop.inria.fr/tropics/>). The current version of WAP-1D-VAR (v1.0) is available from the project website:
<https://zenodo.org/record/4470034> under the Creative Commons Attribution 4.0 International license. The exact version of the
model used to produce the results, input data, and scripts to run the model and produce the plots for all the simulations presented
515 in this paper are archived on Zenodo (Kim, H. Heather, Luo, Ya-Wei, Ducklow, Hugh W., Schofield, Oscar M., Steinberg,
Deborah K., & Doney, Scott C. (2021, January 26). WAP-1D-VAR v1.0: A One-Dimensional Variational Data Assimilation
Model for the West Antarctic Peninsula (Version v1.0). Zenodo. <http://doi.org/10.5281/zenodo.4470034>). A user manual is
available as a separate supplement to this article.

520 Author contributions



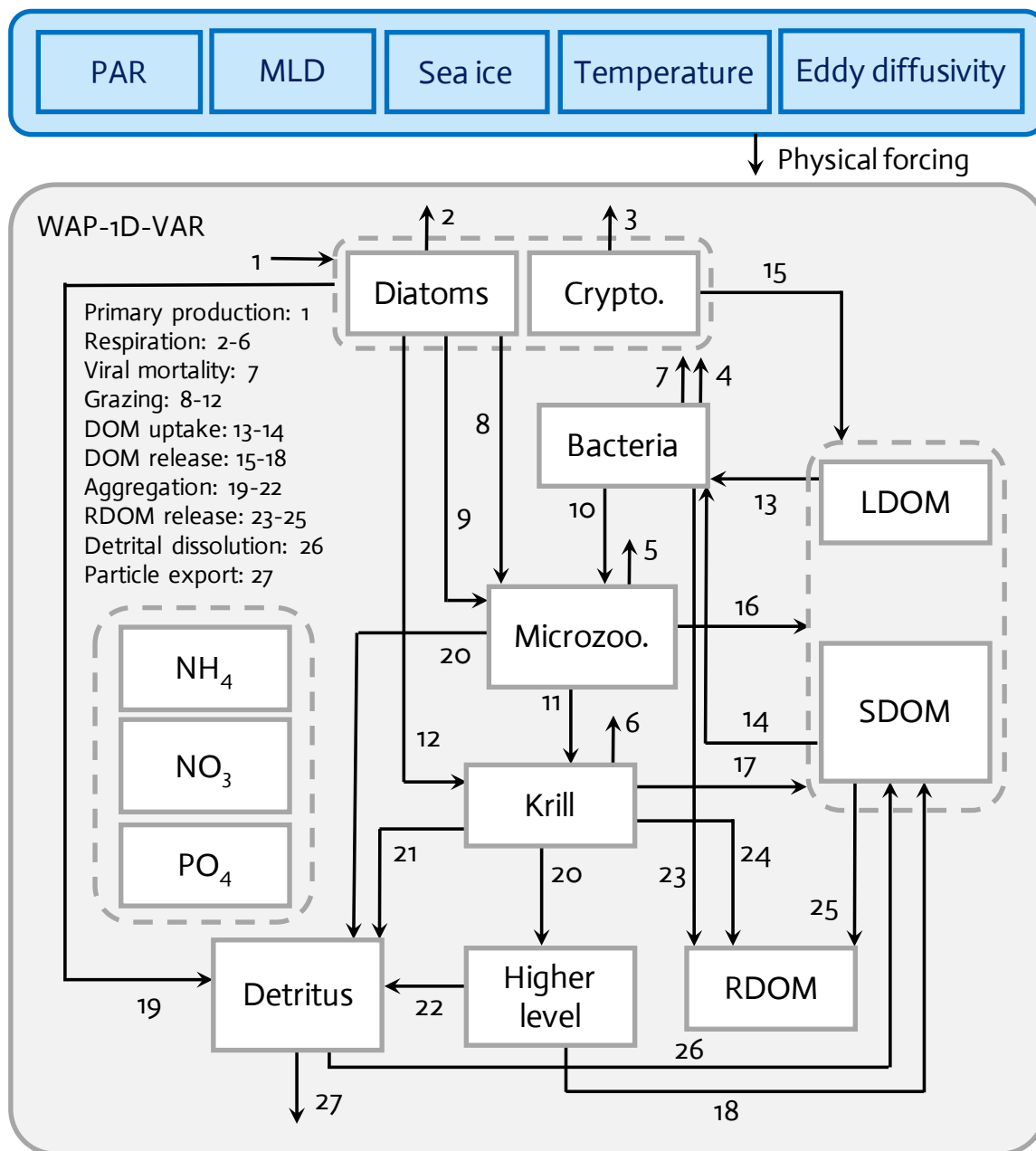
HHK developed the model, performed model simulations, and wrote the manuscript. YWL contributed to model simulations. HWD, OMS, and DKS provided observational data. SCD supervised the research and significantly the manuscript.

Competing interest

525 The authors declare that they have no conflict of interest.



Figure 1. Ecosystem model. The model is forced by five different physical forcing, denoted as a horizontal row across the top of the schematic. The ecosystem component incorporates eleven different prognostic state variables.



PAR: photosynthetically active radiation, MLD: mixed layer depth, Crypto: cryptophytes, Microzoo: microzooplankton, LDOM: labile dissolved organic matter, SDOM: semi-labile dissolved organic matter, RDOM: refractory dissolved organic matter



Figure 2. Variational data assimilation. A variational adjoint scheme is employed for the parameter optimization and data assimilation processes (adapted from Glover et al., 2011). Gradient: the sensitivity of the total cost function with respect to model parameter from optimization.

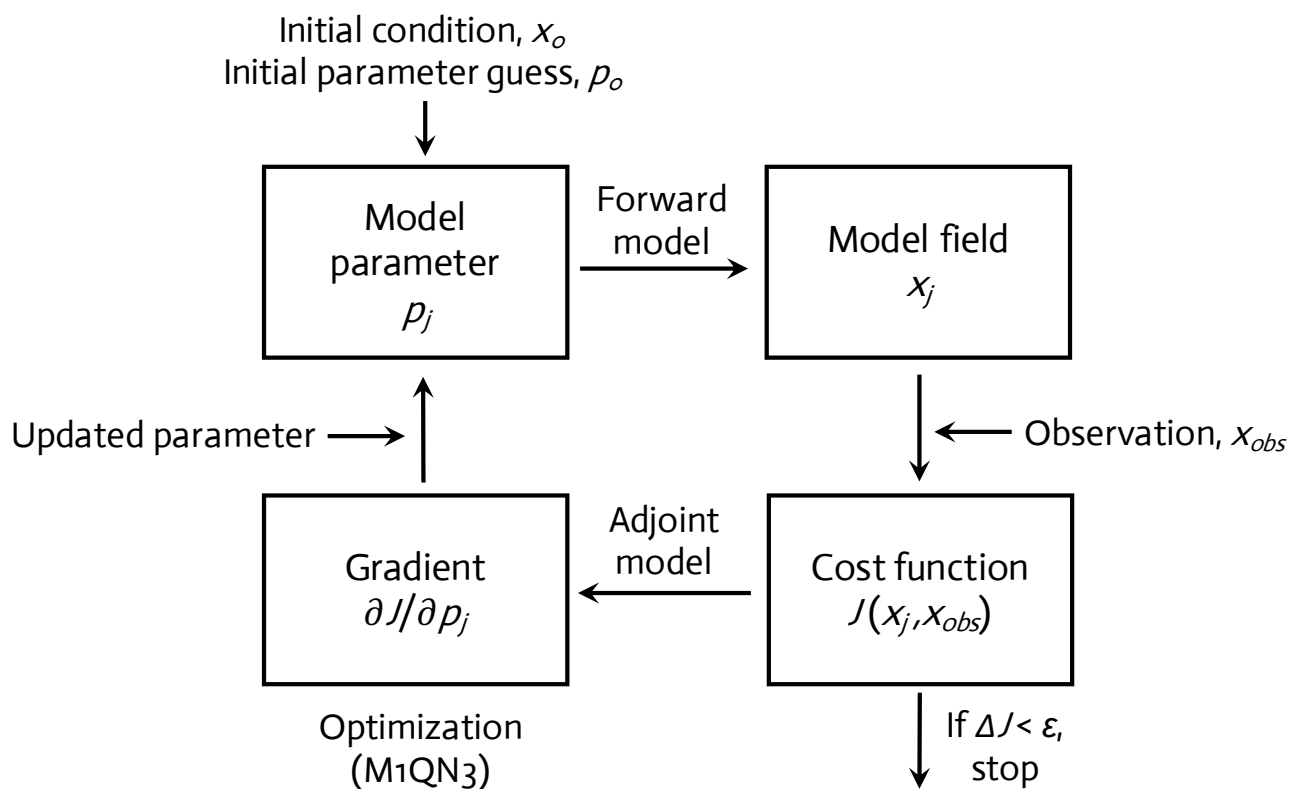
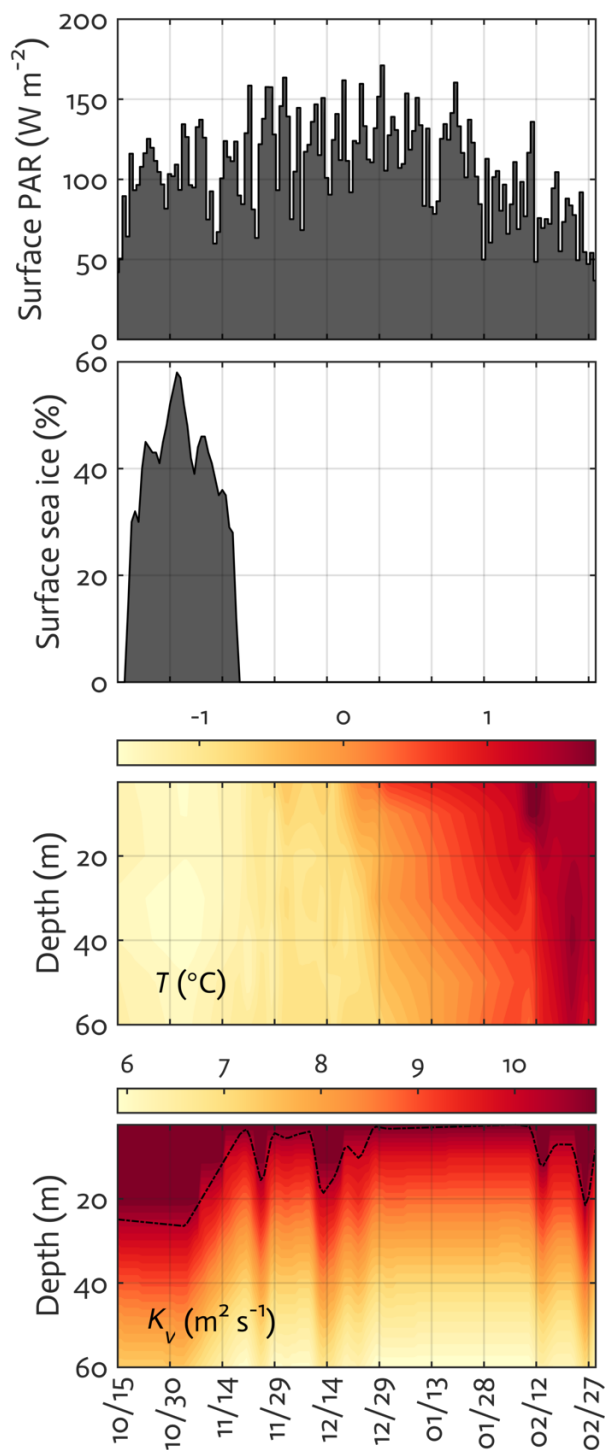




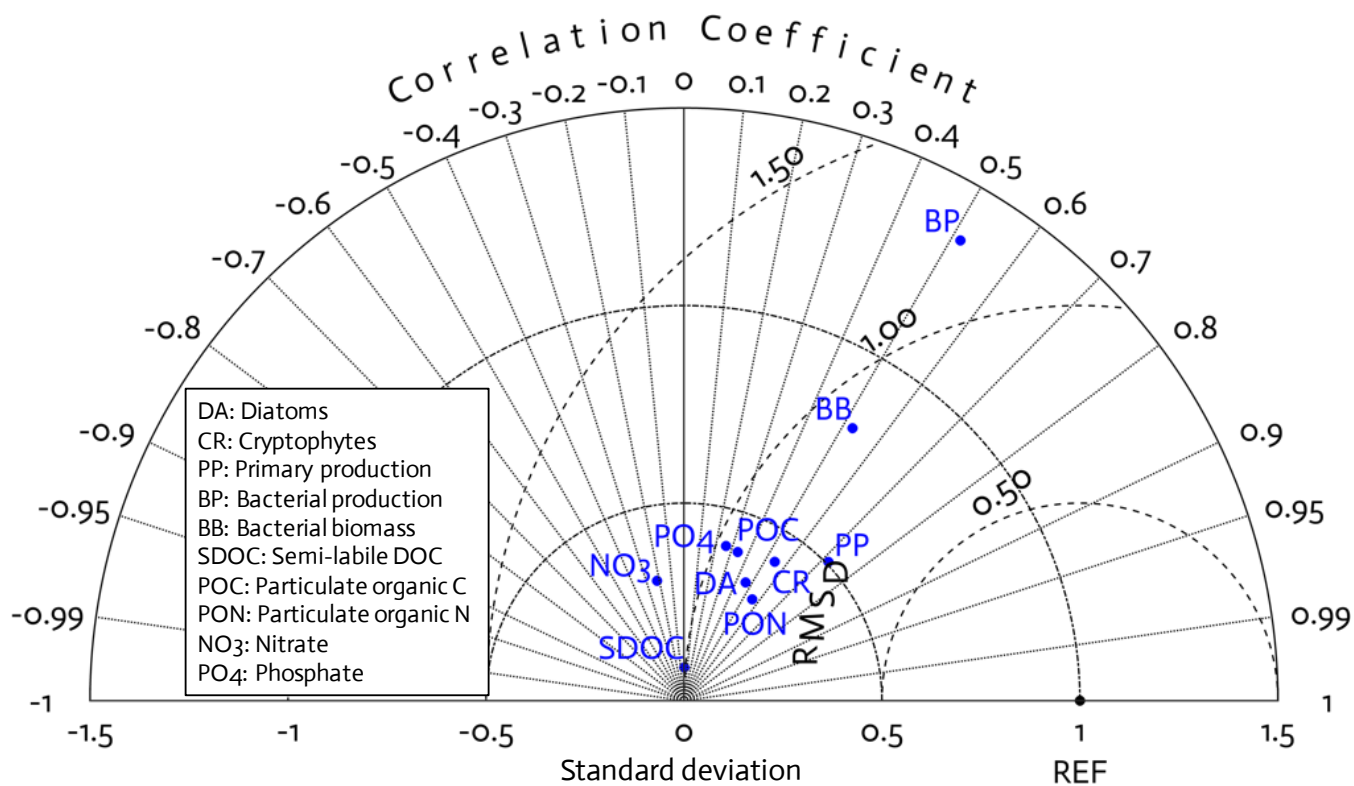
Figure 3. Physical forcing. Physical forcing used in the model, including surface PAR (a), sea ice concentration (b), water temperature (c), and vertical eddy diffusivity (d) overlaid with MLD (dash line) in the modelled growth season.





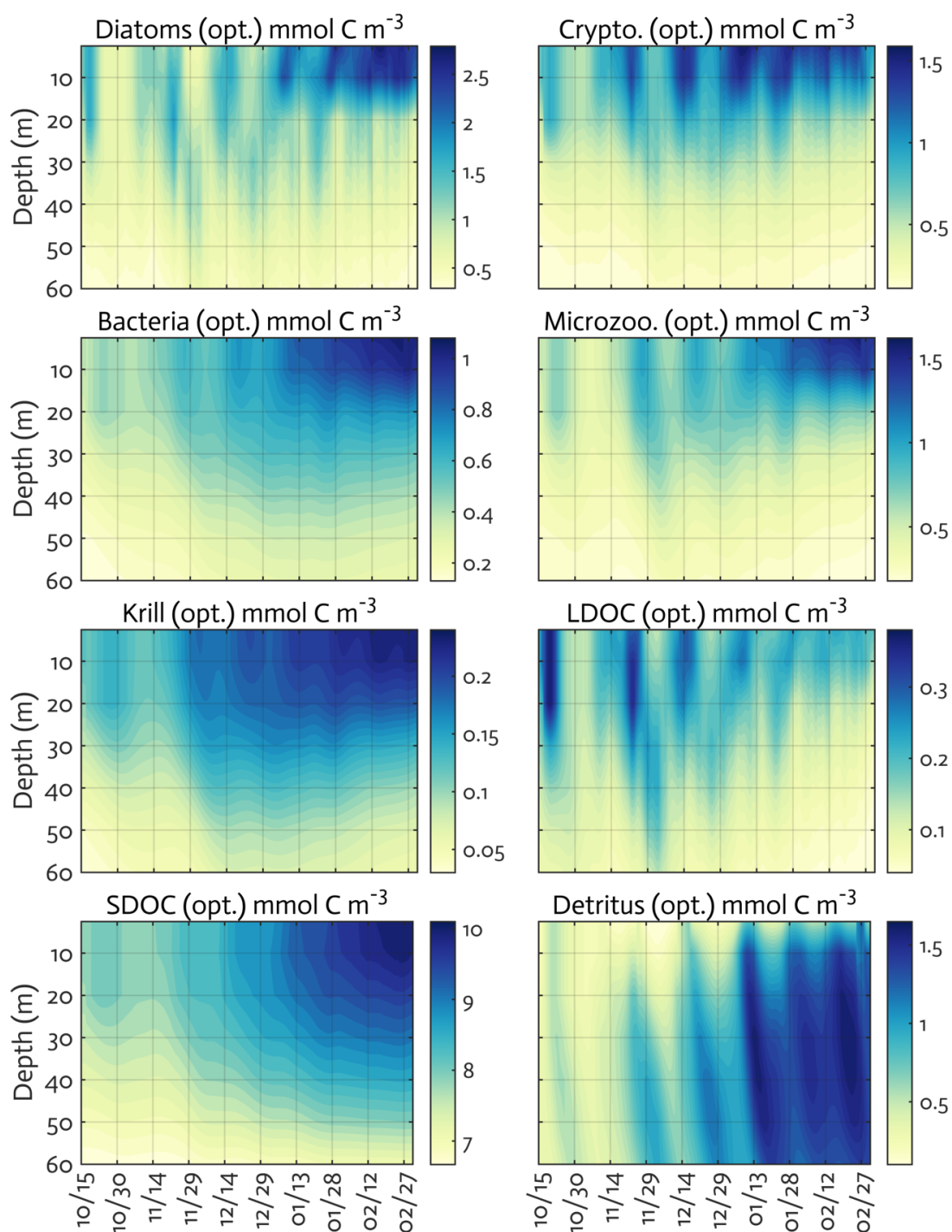
545

Figure 4. Model validation. A Taylor diagram using a polar-coordinate system summarizing the model-observational correspondence for each model stock and flow for the modelled growth season. The angular coordinate for the Pearson correlation coefficient (r), the distance from the origin for the standard deviation normalized by the standard deviation of the observation, and the distance from point (1,0), marked as REF on x-axis, for the centred (bias removed) root-mean-square difference (RMSD) between model results and observations.





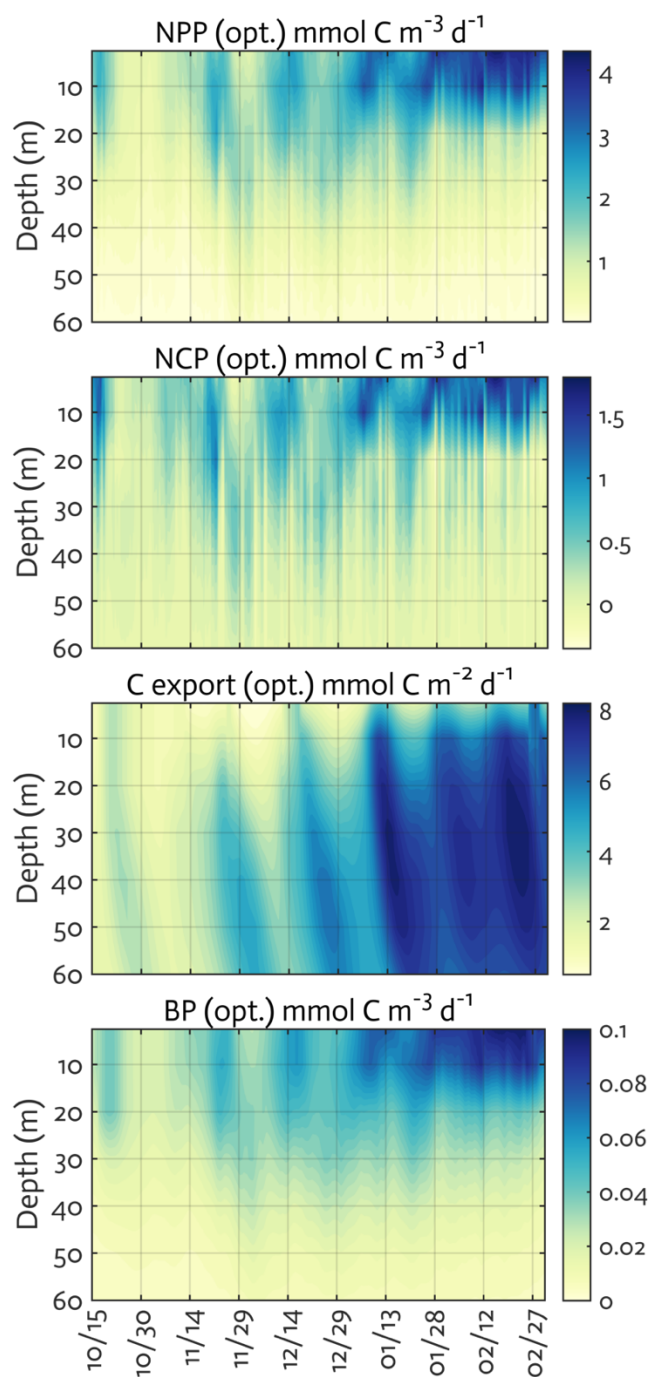
550 **Figure 5. Model state variables.** The model state variables for the modelled growth season (x-axis; month/day). The error (standard deviation) of each model state variable from the Monte Carlo experiments ($N = 1,000$) is available in Figure SX. Note different contour scales among panels. opt. as the optimized model output.





555

Figure 6. Model ecosystem indices. The key ecosystem indices for the modelled growth season (x-axis; month/day). NPP: net primary production, NCP: net community production, C export flux: particulate organic carbon (POC) export flux, and BP: bacterial production. The error (standard deviation) of each rate process from the Monte Carlo experiments ($N = 1,000$) is available in Figure B5. Note different contour scales among panels. opt. as the optimized model output.





560 **Figure 7. Mean carbon stocks and flows.** Depth-integrated (0-60 m) C stocks (mmol C m⁻³), flows (mmol C m⁻³ d⁻¹), and POC export flux at 60-m (mmol C m⁻² d⁻¹) averaged over the modelled Austral growth season (October-March). Values in parentheses as errors propagated from season-averaging and depth-integration of the Monte Carlo errors.

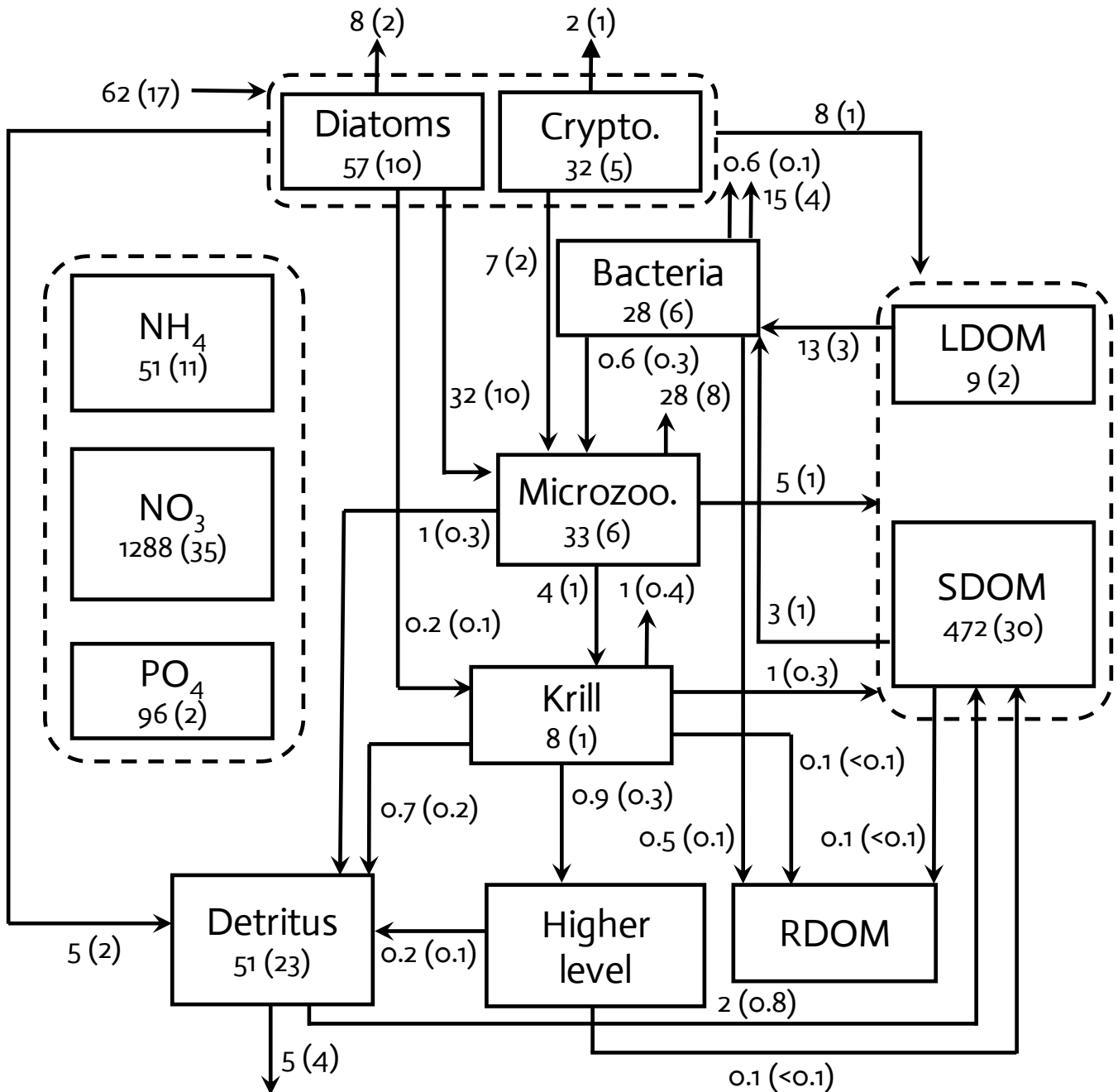




Table 1. Data types, observed means, coefficient of variation, target errors, and costs before and after optimization.

565 The observed mean (\bar{a}), coefficient of variation (CV), and target error (σ) of each assimilated data type used for calculating
 the cost function before and after optimization. J_0 is the normalized cost function before optimization and J_f is the normalized
 cost function after optimization (Eq. 5-6). Data type units: mmol m⁻³ for NO₃, PO₄; mmol C m⁻³ for microzooplankton biomass,
 diatom Chl, cryptophyte Chl, bacterial biomass, SDOC, and POC; mmol N m⁻³ for PON; and mmol C m⁻³ d⁻¹ for PP and BP.
 570 The average error or bias (ϵ_{bias}) is calculated from Stow et al. (2009), where a positive value indicates the model overestimation
 of the observation and vice versa.

| Data types | n | \bar{a} | CV | σ | J_0 | J_f | ϵ_{bias} |
|-------------------------------|-----|-----------|------|----------|-------|-------|-------------------|
| NO ₃ | 75 | 21.54 | 0.04 | 0.80 | 0.76 | 1.01 | -35.86 |
| PO ₄ | 75 | 1.43 | 0.03 | 0.05 | 0.54 | 0.39 | 0.36 |
| log ₁₀ diatom Chl | 86 | -0.07 | 0.20 | 0.08 | 5.47 | 1.05 | -0.75 |
| log ₁₀ crypto. Chl | 86 | -0.27 | 0.24 | 0.10 | 4.34 | 0.43 | -0.59 |
| log ₁₀ PP | 92 | 1.30 | 0.50 | 0.21 | 0.88 | 0.42 | 14.16 |
| Bacterial biomass | 55 | 0.44 | 0.08 | 0.04 | 9.03 | 1.17 | -0.96 |
| BP | 55 | 0.05 | 0.16 | 0.01 | 0.35 | 0.26 | 0.65 |
| SDOC | 55 | 11.39 | 0.20 | 2.30 | 0.68 | 0.75 | -45.23 |
| POC | 91 | 19.78 | 0.13 | 2.58 | 0.50 | 0.45 | -22.17 |
| PON | 91 | 2.66 | 0.12 | 0.32 | 0.67 | 0.64 | -3.49 |
| Total cost function | | | | | 23.21 | 6.57 | |

575



Table 2. Summary of model parameters. Summary of the model parameter symbol and definition, initial guess (p_0) and optimized values (p_f) for optimizable parameters, the cost function gradient with regard to the optimized parameter ($\partial J/\partial p$), and prescribed values for fixed model parameters over the course of simulations. The parameter with ‘n/a’ in the parenthesis is an updated parameter, while the parameter with values in the parenthesis is an optimized parameter with its upper and lower bounds in the parenthesis. The uncertainties for these upper and lower bounds are calculated as: $p_f \times e^{\pm\sigma_f}$ where p_f is the value of the optimized parameter and σ_f is the square roots of diagonal elements of the inverse of the Hessian matrix. The cost function gradient with regard to the optimized parameter ($\partial J/\partial p$) after data assimilation defined as: $\Delta J/e^{\Delta p}$ where $e^{\Delta p} \approx \Delta p$ for an infinitely small Δp . For example, a 10% change of a parameter ($\Delta p = 10\%$) leads to a total cost change equivalent to 10% of the corresponding gradient.

| Model parameter symbol and definition (optimizable) | p_0 | p_f | $\partial J/\partial p$ |
|---|--------|------------------|-------------------------|
| A_E , Arrhenius parameter for temperature function | 4000 | - | -7.8 |
| μ_{DA} , Diatom C-specific maximum growth rate, d^{-1} | 3.5 | - | 6.5 |
| μ_{CR} , Crypto. C-specific maximum growth rate, d^{-1} | 3.0 | - | 1.2 |
| α_{DA} , Initial slope of P-I curve of diatoms, $\text{mol C (g Chl)}^{-1} d^{-1} (\text{W m}^{-2})^{-1}$ | 0.24 | 0.40 (n/a) | <-0.1 |
| α_{CR} , Initial slope of P-I curve of crypto., $\text{mol C (g Chl)}^{-1} d^{-1} (\text{W m}^{-2})^{-1}$ | 0.12 | 0.05 (n/a) | 1.6 |
| β_{DA} , Light inhibition parameter for diatom photosynthesis $(\text{W m}^{-2})^{-1}$ | 0.005 | - | -2.1 |
| β_{CR} , Light inhibition parameter for crypto. photosynthesis $(\text{W m}^{-2})^{-1}$ | 0.005 | - | -0.67 |
| $v_{REF,DA}^N$, Maximum N uptake rate per diatom C biomass, $\text{mol N (mol C)}^{-1} d^{-1}$ | 0.5 | - | 0.10 |
| $v_{REF,CR}^N$, Maximum N uptake rate per crypto. C biomass, $\text{mol N (mol C)}^{-1} d^{-1}$ | 0.3 | - | <0.1 |
| $k_{DA}^{NH_4}$, NH_4 half-saturation concentration for diatom uptake, mmol m^{-3} | 0.1 | - | 0.91 |
| $k_{CR}^{NH_4}$, NH_4 half-saturation concentration for crypto. uptake, mmol m^{-3} | 0.1 | - | 0.31 |
| $k_{DA}^{NO_3}$, NO_3 half-saturation concentration for diatom uptake, mmol m^{-3} | 1.0 | - | -0.91 |
| $k_{CR}^{NO_3}$, NO_3 half-saturation concentration for crypto. uptake, mmol m^{-3} | 0.6 | - | -0.31 |
| $v_{REF,DA}^P$, Maximum P uptake rate per diatom C biomass, $\text{mol P (mol C)}^{-1} d^{-1}$ | 0.03 | - | -0.57 |
| $v_{REF,CR}^P$, Maximum P uptake rate per crypto. C biomass, $\text{mol P (mol C)}^{-1} d^{-1}$ | 0.03 | - | -0.13 |
| $k_{DA}^{PO_4}$, PO_4 half-saturation concentration for diatom uptake, mmol m^{-3} | 0.05 | - | <0.1 |
| $k_{CR}^{PO_4}$, PO_4 half-saturation concentration for crypto. uptake, mmol m^{-3} | 0.04 | - | <0.1 |
| ζ^{NO_3} , C requirement (respiration) to assimilate NO_3 , $\text{mol C (mol N)}^{-1}$ | 2.0 | - | -1.3 |
| θ , Maximum Chl/N ratio, $\text{g Chl } a (\text{mol N})^{-1}$ | 2.9 | 3.16 (n/a) | 1.6 |
| $ex_{PSV,DA}$, Diatom passive excretion rate per biomass, d^{-1} | 0.05 | - | -0.54 |
| $ex_{PSV,CR}$, Crypto. passive excretion rate per biomass, d^{-1} | 0.05 | - | 1.0 |
| $ex_{ACT,DA}$, Diatom active excretion rate per growth rate, d^{-1} | 0.05 | - | -0.11 |
| $ex_{ACT,CR}$, Crypto. active excretion rate per growth rate, d^{-1} | 0.05 | - | 0.18 |
| pom_{DA} , POM production rate by diatom aggregation, $(\text{mmol C m}^{-3})^{-1} d^{-1}$ | 0.04 | - | -1.0 |
| pom_{CR} , POM production rate by crypto. aggregation, $(\text{mmol C m}^{-3})^{-1} d^{-1}$ | 0.03 | - | -0.56 |
| k^{DOC} , DOC half-saturation concentration for bacterial uptake, mmol C m^{-3} | 0.65 | - | -0.24 |
| r_{SDOM} , Parameter controlling SDOM lability | 0.005 | - | 0.31 |
| μ_{BAC} , Maximum bacterial growth rate, d^{-1} | 2.0 | 5.17 (n/a) | 0.96 |
| $b_{R,BAC}$, Parameter control bacterial active respiration rate versus production, $(\text{mmol C m}^{-3} d^{-1})^{-1}$ | 0.015 | - | 0.44 |
| $ex_{ADJ,BAC}$, Bacterial extra SDOC excretion rate, d^{-1} | 2.0 | - | <0.1 |
| $remi_{BAC}$, Bacterial nutrient regeneration rate, d^{-1} | 6.0 | - | 0.26 |
| $ex_{REFR,BAC}$, Bacterial RDOC production rate, d^{-1} | 0.017 | - | 4.3 |
| f_s , Bacterial selection strength on SDOM | 0.25 | - | <-0.1 |
| r_{BAC}^B , Bacterial basal respiration rate, d^{-1} | 0.0127 | - | 0.90 |
| $r_{min,BAC}^A$, Bacterial minimum active respiration rate, d^{-1} | 0.035 | - | <-0.1 |
| $r_{max,BAC}^A$, Bacterial maximum active respiration rate, d^{-1} | 0.58 | 0.89 (0.88-0.90) | <0.1 |
| $mori_{BAC}$, Bacterial mortality rate, d^{-1} | 0.02 | - | 4.6 |
| μ_{MZ} , Microzoo. C-specific maximum growth rate, d^{-1} | 2.5 | 6.30 (n/a) | <-0.1 |
| g_{DA} , Diatom half-saturation concentration in microzoo. grazing, mmol C m^{-3} | 1.0 | 1.28 (1.15-1.42) | <0.1 |
| g'_{DA} , Diatom half-saturation concentration in krill grazing, mmol C m^{-3} | 1.0 | 3.65 (n/a) | 0.15 |



| | | | |
|--|-----------------------|------------------|-------|
| g_{CR} , Crypto. half-saturation concentration in microzoo. grazing, mmol C m^{-3} | 1.0 | 1.83 (1.60-2.09) | <0.1 |
| g_{BAC} , Bacterial half-saturation concentration in microzoo. grazing, mmol C m^{-3} | 0.55 | 5.25 (n/a) | -4.3 |
| ex_{MZ} , Total DOM excretion rate per microzoo. gross growth, d^{-1} | 0.15 | - | 1.4 |
| $f_{ex,MZ}$, Fraction of LDOC of total microzoo. DOC excretion | 0.75 | - | 4.1 |
| r_{MZ}^B , Microzoo. basal respiration rate, d^{-1} | 0.01 | - | <0.1 |
| r_{MZ}^A , Microzoo. active respiration rate, d^{-1} | 0.42 | 0.71 (0.70-0.72) | <0.1 |
| $ex_{ADJ,MZ}$, Microzoo. extra SDOM excretion rate, d^{-1} | 2.0 | - | 0 |
| $remi_{MZ}$, Microzoo. nutrient regeneration rate, d^{-1} | 4.68 | - | 0.26 |
| pom_{MZ} , POM production rate per microzoo. gross growth, d^{-1} | 0.027 | - | -0.20 |
| μ_{KR} , Maximum krill C-specific growth rate, d^{-1} | 1.2 | 2.11 (2.03-2.19) | <0.1 |
| g_{MZ} , Microzoo. half-saturation concentration in krill grazing, mmol C m^{-3} | 1.0 | 0.47 (n/a) | <-0.1 |
| ex_{KR} , Total DOM excretion rate per krill gross growth, d^{-1} | 0.3 | - | -0.88 |
| $f_{ex,KR}$, Fraction of labile DOC of total krill DOC excretion | 0.75 | - | 1.0 |
| r_{KR}^B , Krill basal respiration rate, d^{-1} | 0.03 | - | <-0.1 |
| r_{KR}^A , Krill active respiration rate, d^{-1} | 0.3 | - | -0.79 |
| $ex_{ADJ,KR}$, Krill extra SDOM excretion rate, d^{-1} | 2.0 | - | <0.1 |
| $remi_{KR}$, Krill nutrient regeneration rate, d^{-1} | 4.0 | - | <0.1 |
| pom_{KR} , POM production rate per krill gross growth, d^{-1} | 0.15 | - | -0.55 |
| $ex_{REFR,KR}$, Krill RDOC production rate, d^{-1} | 0.02 | - | <-0.1 |
| $remv_{KR}$, Krill removal rate by higher-trophic levels, $(\text{mmol C m}^{-3})^{-1} \text{d}^{-1}$ | 0.78 | - | 0.59 |
| f_{KR} , Fraction of SDOM production by krill | 0.1 | - | <-0.1 |
| $f_{POM,HZ}$, Fraction of POM production by higher-trophic level | 0.2 | - | <-0.1 |
| $ex_{REFR,SDOM}$, Conversion rate of SDOM to RDOM, d^{-1} | 9.0E-4 | - | 0.10 |
| $q_{N,RDOM}^C$, RDOM N/C ratio, $\text{mol N (mol C)}^{-1}$ | 0.05 | - | 0.40 |
| $q_{P,RDOM}^C$, RDOM P/C ratio, $\text{mol P (mol C)}^{-1}$ | 6.5E-4 | - | <-0.1 |
| $q_{N,POM}^C$, N/C ratio for POM production by microzoo. and krill, $\text{mol N (mol C)}^{-1}$ | 0.12 | - | 0.63 |
| $q_{P,POM}^C$, P/C ratio for POM production by microzoo. and krill, $\text{mol P (mol C)}^{-1}$ | 4.5E-3 | - | -0.31 |
| r_{nrf} , Nitrification rate (NH_4 to NO_3), d^{-1} | 0.076 | - | -2.7 |
| prf_N , Preference for dissolving N content in POM | 1.1 | - | <-0.1 |
| prf_P , Preference for dissolving P content in POM | 4.0 | - | 0.30 |
| w_{NSV} , Detritus vertical sinking velocity, m d^{-1} | 5.0 | - | 2.3 |
| di_{SS} , Detrital dissolution rate, d^{-1} | 0.14 | 0.03 (n/a) | -0.69 |
| Model parameter symbol and definition (fixed) | p | | |
| T_{ref} , Reference temperature in Arrhenius function, $^{\circ}\text{C}$ | 15 | | |
| $q_{N,MIN,DA}^C$, Minimum N/C ratio of diatoms | 0.034 | | |
| $q_{N,MAX,DA}^C$, Maximum N/C ratio of diatoms | 0.17 | | |
| $q_{N,RDF,DA}^C$, Reference (Redfield) N/C ratio of diatoms | 0.15 | | |
| $q_{P,MIN,DA}^C$, Minimum P/C ratio of diatoms | 0.0019 | | |
| $q_{P,MAX,DA}^C$, Maximum P/C ratio of diatoms | 0.0169 | | |
| $q_{P,RDF,DA}^C$, Reference (Redfield) P/C ratio of diatoms | 0.0094 | | |
| $q_{N,MIN,CR}^C$, Minimum N/C ratio of crypto. | 0.034 | | |
| $q_{N,MAX,CR}^C$, Maximum N/C ratio of crypto. | 0.17 | | |
| $q_{N,RDF,CR}^C$, Reference (Redfield) N/C ratio of crypto. | 0.15 | | |
| $q_{P,MIN,CR}^C$, Minimum P/C ratio of crypto. | 0.0019 | | |
| $q_{P,MAX,CR}^C$, Maximum P/C ratio of crypto. | 0.0169 | | |
| $q_{P,RDF,CR}^C$, Reference (Redfield) P/C ratio of crypto. | 0.0094 | | |
| $q_{N,BAC}^C$, Reference (optimal) N/C ratio of bacteria | 0.18 | | |
| $q_{P,BAC}^C$, Reference (optimal) P/C ratio of bacteria | 0.02 | | |
| $q_{N,MZ}^C$, Reference (optimal) N/C ratio of microzoo. | 0.20 | | |
| $q_{P,MZ}^C$, Reference (optimal) P/C ratio of microzoo. | 0.022 | | |
| $q_{N,KR}^C$, Reference (optimal) N/C ratio of krill | 0.20 | | |
| $q_{P,KR}^C$, Reference (optimal) P/C ratio of krill | 0.008 | | |



| | |
|--|-------|
| ϵ_{DA} , Grazing limit to the amount of diatoms available for microzoo. grazing, mmol C m^{-3} | 0.001 |
| ϵ_{CR} , Grazing limit to the amount of crypto. available for microzoo. grazing, mmol C m^{-3} | 2.949 |



590 Appendix A

1. Temperature effect

$$T_f = \exp\{-A_E \times (1/T - 1/T_{ref})\} \quad (\text{A.1.1})$$

2. Diatom processes

- Cellular quota (ratio):

$$595 \quad Q_{N,DA}^C = N_{DA}/C_{DA} \quad (\text{A.2.1})$$

$$Q_{P,DA}^C = P_{DA}/C_{DA} \quad (\text{A.2.2})$$

$$Q_{CHL,DA}^C = CHL_{DA}/C_{DA} \quad (\text{A.2.3})$$

- N and P limitation function:

$$600 \quad N_{f,DA} = (Q_{N,DA}^C - q_{N,MIN,DA}^C)/(q_{N,RDF,DA}^C - q_{N,MIN,DA}^C) \quad 0 \leq N_{f,DA} \leq 1 \quad (\text{A.2.4})$$

$$P_{f,DA} = (Q_{P,DA}^C - q_{P,MIN,DA}^C)/(q_{P,RDF,DA}^C - q_{P,MIN,DA}^C) \quad 0 \leq P_{f,DA} \leq 1 \quad (\text{A.2.5})$$

- Maximum photosynthesis rate:

$$P_{MAX}^C = \mu_{DA} \times T_f \times \min(N_{f,DA}, P_{f,DA}) \quad (\text{A.2.6})$$

- C-specific gross primary production:

$$G_{DA}^C = C_{DA} \times P_{MAX}^C \times \{1 - \exp(-\alpha_{DA} \times Q_{CHL}^C \times PAR)/P_{MAX}^C\} \times \exp(-\beta_{DA} \times PAR) \quad (\text{A.2.7})$$

- Limitation on N and P uptake:

$$605 \quad V_{MAX}^N = (q_{N,MAX}^C - Q_{N,DA}^C)/(q_{N,MAX}^C - q_{N,RDF}^C) \quad 0 \leq V_{MAX}^N \leq 1 \quad (\text{A.2.8})$$

$$V_{MAX}^P = (q_{P,MAX}^C - Q_{P,DA}^C)/(q_{P,MAX}^C - q_{P,RDF}^C) \quad 0 \leq V_{MAX}^P \leq 1 \quad (\text{A.2.9})$$

- N assimilation:

$$610 \quad G_{DA}^{NH4} = C_{DA} \times V_{REF}^N \times T_f \times V_{MAX}^N \times \{NH4/(NH4 + k^{NH4} + NO3 \times k^{NH4}/k^{NO3})\} \quad (\text{A.2.10})$$

$$G_{DA}^{NO3} = C_{DA} \times V_{REF}^N \times T_f \times V_{MAX}^N \times \{NO3/(NO3 + k^{NO3} + NH4 \times k^{NO3}/k^{NH4})\} \quad (\text{A.2.11})$$

$$G_{DA}^N = G_{DA}^{NH4} + G_{DA}^{NO3} \quad (\text{A.2.12})$$

- P assimilation:

$$G_{DA}^{PO4} = C_{DA} \times V_{REF}^P \times T_f \times V_{MAX}^P \times \{PO4/(PO4 + k^{PO4})\} \quad (\text{A.2.13})$$

- Chlorophyll production:

$$615 \quad G_{DA}^{CHL} = \theta \times (G_{DA}^{NH4} + G_{DA}^{NO3}) \times \{G_{DA}^C / \alpha \times CHL_{DA} \times PAR \times \exp(-\beta \times PAR)\} \quad (\text{A.2.14})$$

- Respiration:

$$R_{DA}^C = G_{DA}^{NO3} \times \zeta^{NO3} \quad (\text{A.2.15})$$

- Passive excretion of LDOM:

$$620 \quad E_{DA,LDOP,PSV}^C = ex_{DA,PSV} \times C_{DA} \quad (\text{A.2.16})$$

$$E_{DA,LDOC,PSV}^N = ex_{DA,PSV} \times N_{DA} \quad (\text{A.2.17})$$

$$E_{DA,LDOC,PSV}^P = ex_{DA,PSV} \times P_{DA} \quad (\text{A.2.18})$$

- Active excretion of LDOC:

$$E_{DA,LDOC,ACT}^C = ex_{DA,ACT} \times G_{DA}^C \quad (\text{A.2.19})$$

- Active excretion of SDOC:

$$625 \quad E_{DA,SDOC,ACT}^C = 0.5 \times C_{DA} \times \max(1 - Q_{N,DA}^C/q_{N,RDF,DA}^C, 1 - Q_{P,DA}^C/q_{P,RDF,DA}^C, 0) \quad (\text{A.2.20})$$

- Active excretion of SDON and SDOP (if $EX_{DA,SDOC,ACT}^C > 0$, otherwise 0):

$$E_{DA,SDON,ACT}^N = 0.5 \times 0.25 \times N_{DA} \times \max(1 - Q_{P,DA}^C/q_{P,RDF,DA}^C/q_{N,RDF,DA}^C, 0) \quad (\text{A.2.21})$$

$$E_{DA,SDOP,ACT}^P = 0.5 \times 0.25 \times P_{DA} \times \max(1 - Q_{N,DA}^C/q_{N,RDF,DA}^C/q_{P,RDF,DA}^C, 0) \quad (\text{A.2.22})$$



- 630 • Partitioning between LDOM and SDOM:

$$E_{DA,LDOC}^C = E_{DA,LDOC,PSV}^C + 0.75 \times E_{DA,LDOC,ACT}^C \quad (A.2.23)$$

$$E_{DA,LDON}^N = E_{DA,LDON,PSV}^N \quad (A.2.24)$$

$$E_{DA,LDOP}^P = E_{DA,LDOP,PSV}^P \quad (A.2.25)$$

$$E_{DA,SDOC}^C = E_{DA,SDOC,ACT}^C + 0.25 \times E_{DA,LDOC,ACT}^C \quad (A.2.26)$$

$$E_{DA,SDON}^N = E_{DA,SDON,ACT}^N \quad (A.2.27)$$

635
$$E_{DA,SDOP}^P = E_{DA,SDOP,ACT}^P \quad (A.2.28)$$
- POM production by aggregation:

$$D_{DA}^C = pom_{DA} \times C_{DA} \times C_{DA} \quad (A.2.29)$$

$$D_{DA}^N = Q_{N,DA}^C \times D_{DA}^C \quad (A.2.30)$$

$$D_{DA}^P = Q_{P,DA}^C \times D_{DA}^C \quad (A.2.31)$$

640
$$D_{DA}^{CHL} = Q_{CHL,DA}^C \times D_{DA}^C \quad (A.2.32)$$
- Grazing by microzooplankton:

$$GZ_{DA,MZ}^C = T_f \times \mu_{MZ} \times C_{MZ} \times [(C_{DA} - \epsilon_{DA})^2 / \{ (C_{DA} - \epsilon_{DA})^2 + g_{DA}^2 + (C_{CRYPTO} \times g_{DA}/g_{CRYPTO})^2 + (C_{BAC} \times g_{DA}/g_{BAC})^2 \}] \quad (A.2.33)$$

$$GZ_{DA,MZ}^N = Q_{N,DA}^C \times GZ_{DA,MZ}^C \quad (A.2.34)$$

645
$$GZ_{DA,MZ}^P = Q_{P,DA}^C \times GZ_{DA,MZ}^C \quad (A.2.35)$$

$$GZ_{DA,MZ}^{CHL} = Q_{CHL,DA}^C \times GZ_{DA,MZ}^C \quad (A.2.36)$$
- Grazing by krill:

$$GZ_{DA,KR}^C = T_f \times \mu_{KR} \times C_{KR} \times [C_{DA}^2 / \{ C_{DA}^2 + g'_{DA}{}^2 + (C_{MZ} \times g'_{DA}/g_{MZ})^2 \}] \quad (A.2.37)$$

650
$$GZ_{DA,KR}^N = Q_{N,DA}^C \times GZ_{DA,KR}^C \quad (A.2.38)$$

$$GZ_{DA,KR}^P = Q_{P,DA}^C \times GZ_{DA,KR}^C \quad (A.2.39)$$

$$GZ_{DA,KR}^{CHL} = Q_{CHL,DA}^C \times GZ_{DA,KR}^C \quad (A.2.40)$$
- The net growth rate equations:

$$\frac{dC_{DA}}{dt} = G_{DA}^C - E_{DA,LDOC}^C - E_{DA,SDOC}^C - D_{DA}^C - R_{DA}^C - GZ_{DA,MZ}^C - GZ_{DA,KR}^C \quad (A.2.41)$$

655
$$\frac{dN_{DA}}{dt} = G_{DA}^N - E_{DA,LDON}^N - E_{DA,SDON}^N - D_{DA}^N - GZ_{DA,MZ}^N - GZ_{DA,KR}^N \quad (A.2.42)$$

$$\frac{dP_{DA}}{dt} = G_{DA}^P - E_{DA,LDOP}^P - E_{DA,SDOP}^P - D_{DA}^P - GZ_{DA,MZ}^P - GZ_{DA,KR}^P \quad (A.2.43)$$

$$\frac{dCHL_{DA}}{dt} = G_{DA}^{CHL} - D_{DA}^{CHL} - GZ_{DA,MZ}^{CHL} - GZ_{DA,KR}^{CHL} \quad (A.2.44)$$

3. Cryptophyte processes

- 660 • Cellular quota (ratio):

$$Q_{N,CR}^C = N_{CR}/C_{CR} \quad (A.3.1)$$

$$Q_{P,CR}^C = P_{CR}/C_{CR} \quad (A.3.2)$$

$$Q_{CHL,CR}^C = CHL_{CR}/C_{CR} \quad (A.3.3)$$
- N and P limitation function:

$$N_{f,CR} = (Q_{N,CR}^C - q_{N,MIN,CR}^C) / (q_{N,RDF,CR}^C - q_{N,MIN,CR}^C) \quad 0 \leq N_{f,CR} \leq 1 \quad (A.3.4)$$

665
$$P_{f,CR} = (Q_{P,CR}^C - q_{P,MIN,CR}^C) / (q_{P,RDF,CR}^C - q_{P,MIN,CR}^C) \quad 0 \leq P_{f,CR} \leq 1 \quad (A.3.5)$$



- Maximum primary production rate:

$$P_{MAX}^C = \mu_{CR} \times T_f \times \min(N_{f,CR}, P_{f,CR}) \quad (\text{A.3.6})$$
- C-specific gross primary production:

$$G_{CR}^C = C_{CR} \times P_{MAX}^C \times \{ 1 - \exp(-\alpha_{CR} \times Q_{CHL}^C \times PAR) / P_{MAX}^C \} \times \exp(-\beta_{CR} \times PAR) \quad (\text{A.3.7})$$
- 670 • Limitation on N and P uptake:

$$V_{MAX}^N = (q_{N,MAX}^C - Q_{N,CR}^C) / (q_{N,MAX}^C - q_{N,RDF}^C) \quad 0 \leq V_{MAX}^N \leq 1 \quad (\text{A.3.8})$$

$$V_{MAX}^P = (q_{P,MAX}^C - Q_{P,CR}^C) / (q_{P,MAX}^C - q_{P,RDF}^C) \quad 0 \leq V_{MAX}^P \leq 1 \quad (\text{A.3.9})$$
- Nitrogen assimilation:

$$G_{CR}^{NH4} = C_{CR} \times V_{REF}^N \times T_f \times V_{MAX}^N \times \{ NH4 / (NH4 + k^{NH4} + NO3 \times k^{NH4} / k^{NO3}) \} \quad (\text{A.3.10})$$

$$G_{CR}^{NO3} = C_{CR} \times V_{REF}^N \times T_f \times V_{MAX}^N \times \{ NO3 / (NO3 + k^{NO3} + NH4 \times k^{NO3} / k^{NH4}) \} \quad (\text{A.3.11})$$

$$G_{CR}^N = G_{CR}^{NH4} + G_{CR}^{NO3} \quad (\text{A.3.12})$$
- Phosphorus assimilation:

$$G_{CR}^{PO4} = C_{CR} \times V_{REF}^P \times T_f \times V_{MAX}^P \times \{ PO4 / (PO4 + k^{PO4}) \} \quad (\text{A.3.13})$$
- 680 • Chlorophyll production:

$$G_{CHL,CR}^C = \theta \times (G_{CR}^{NH4} + G_{CR}^{NO3}) \times \{ G_{CR}^C / \alpha \times CHL_{CR} \times PAR \times \exp(-\beta \times PAR) \} \quad (\text{A.3.14})$$
- Respiration:

$$R_{CR}^C = G_{CR}^{NO3} \times \zeta^{NO3} \quad (\text{A.3.15})$$
- Passive excretion of LDOM:

$$E_{CR,LDOP,PSV}^C = ex_{CR,PSV} \times C_{CR} \quad (\text{A.3.16})$$

$$E_{CR,LDON,PSV}^N = ex_{CR,PSV} \times N_{CR} \quad (\text{A.3.17})$$

$$E_{CR,LDOP,PSV}^P = ex_{CR,PSV} \times P_{CR} \quad (\text{A.3.18})$$
- Active excretion of LDOC:

$$E_{CR,LDOP,ACT}^C = ex_{CR,ACT} \times G_{CR}^C \quad (\text{A.3.19})$$
- Active excretion of SDOC:

$$E_{CR,SDOP,ACT}^C = 0.5 \times C_{CR} \times \max(1 - Q_{N,CR}^C / q_{N,RDF,CR}^C, 1 - Q_{P,CR}^C / q_{P,RDF,CR}^C, 0) \quad (\text{A.3.20})$$
- Active excretion of SDON and SDOP (if $EX_{CR,SDOP,ACT}^C > 0$, otherwise 0):

$$E_{CR,SDON,ACT}^N = 0.5 \times 0.25 \times N_{CR} \times \max(1 - Q_{P,CR}^C / q_{P,RDF,CR}^C, 0) \quad (\text{A.3.21})$$

$$E_{CR,SDOP,ACT}^P = 0.5 \times 0.25 \times P_{CR} \times \max(1 - Q_{N,CR}^C / q_{N,RDF,CR}^C, 0) \quad (\text{A.3.22})$$
- 695 • Partitioning between LDOM and SDOM:

$$E_{CR,LDOP}^C = E_{CR,LDOP,PSV}^C + 0.75 \times E_{CR,LDOP,ACT}^C \quad (\text{A.3.23})$$

$$E_{CR,LDON}^N = E_{CR,LDON,PSV}^N \quad (\text{A.3.24})$$

$$E_{CR,LDOP}^P = E_{CR,LDOP,PSV}^P \quad (\text{A.3.25})$$

$$E_{CR,SDOP}^C = E_{CR,SDOP,ACT}^C + 0.25 \times E_{CR,LDOP,ACT}^C \quad (\text{A.3.26})$$

$$E_{CR,SDON}^N = E_{CR,SDON,ACT}^N \quad (\text{A.3.27})$$

$$E_{CR,SDOP}^P = E_{CR,SDOP,ACT}^P \quad (\text{A.3.28})$$
- 700 • POM production by aggregation:

$$D_{CR}^C = pom_{CR} \times C_{CR} \times C_{CR} \quad (\text{A.3.29})$$

$$D_{CR}^N = Q_{N,CR}^C \times A_{CR}^C \quad (\text{A.3.30})$$

$$D_{CR}^P = Q_{P,CR}^C \times A_{CR}^C \quad (\text{A.3.31})$$

$$D_{CHL,CR}^C = Q_{CHL,CR}^C \times A_{CR}^C \quad (\text{A.3.32})$$
- 705 • Grazing by microzooplankton:

$$GZ_{CR}^C = T_f \times \mu_{MZ} \times C_{MZ}$$



$$\times [(C_{CR} - \epsilon_{CR})^2 / \{ (C_{CR} - \epsilon_{CR})^2 + g_{CR}^2 + (C_{DA} \times g_{CR} / g_{DA})^2 + (C_{BAC} \times g_{CR} / g_{BAC})^2 \}] \quad (\text{A.3.33})$$

$$GZ^N_{CR} = Q^C_{N,CR} \times GZ^C_{CR,MZ} \quad (\text{A.3.34})$$

$$GZ^P_{CR} = Q^C_{P,CR} \times GZ^C_{CR,MZ} \quad (\text{A.3.35})$$

$$GZ^{CHL}_{CR} = Q^C_{CHL,CR} \times GZ^C_{CR,MZ} \quad (\text{A.3.36})$$

- The net growth rate equations:

$$\frac{dC_{CR}}{dt} = G^C_{CR} - E^C_{CR,LDOC} - E^C_{CR,SDOC} - D^C_{CR} - R^C_{CR} - GZ^C_{CR} \quad (\text{A.3.37})$$

$$\frac{dN_{CR}}{dt} = G^N_{CR} - E^N_{CR,LDON} - E^N_{CR,SDON} - D^N_{CR} - GZ^N_{CR} \quad (\text{A.3.38})$$

$$\frac{dP_{CR}}{dt} = G^P_{CR} - E^P_{CR,LDOP} - E^P_{CR,SDOP} - D^N_{CR} - GZ^P_{CR} \quad (\text{A.3.39})$$

$$\frac{dCHL_{CR}}{dt} = G^{CHL}_{CR} - D^{CHL}_{CR} - GZ^{CHL}_{CR} \quad (\text{A.3.40})$$

4. Bacterial processes

- Cellular quota (ratio):

$$Q^C_{N,BAC} = N_{BAC} / C_{BAC} \quad (\text{A.4.1})$$

$$Q^C_{P,BAC} = P_{BAC} / C_{BAC} \quad (\text{A.4.2})$$

$$Q^P_{N,BAC} = N_{BAC} / P_{BAC} \quad (\text{A.4.3})$$

$$Q^C_{N,LDOM} = N_{LDOM} / C_{LDOM} \quad (\text{A.4.4})$$

$$Q^C_{P,LDOM} = P_{LDOM} / C_{LDOM} \quad (\text{A.4.5})$$

$$Q^C_{N,SDOM} = N_{SDOM} / C_{SDOM} \quad (\text{A.4.6})$$

$$Q^C_{P,SDOM} = P_{SDOM} / C_{SDOM} \quad (\text{A.4.7})$$

- N and P limitation function:

$$N_{f,BAC} = Q^C_{N,BAC} / q^C_{N,BAC} \quad 0 \leq N_{f,BAC} \leq 1 \quad (\text{A.4.8})$$

$$P_{f,BAC} = Q^C_{P,BAC} / q^C_{P,BAC} \quad 0 \leq P_{f,BAC} \leq 1 \quad (\text{A.4.9})$$

- Maximum available LDOC and SDOC:

$$ALC = C_{LDOC} \quad (\text{A.4.10})$$

$$ASC = r_{SDOC} \times C_{SDOC} \quad (\text{A.4.11})$$

- Bacterial uptake of LDOC and SDOC (i.e., bacterial gross C growth):

$$G^C_{BAC,LDOC} = \mu_{BAC} \times T_f \times C_{BAC} \times \min(N_{f,BAC}, P_{f,BAC}) \times \{ ALC / (ALC + k^{DOC} + ASC) \} \quad (\text{A.4.12})$$

$$G^C_{BAC,SDOC} = \mu_{BAC} \times T_f \times C_{BAC} \times \min(N_{f,BAC}, P_{f,BAC}) \times \{ ASC / (ASC + k^{DOC} + ALC) \} \quad (\text{A.4.13})$$

$$G^C_{BAC,DOC} = G^C_{BAC,LDOC} + G^C_{BAC,SDOC} \quad (\text{A.4.14})$$

- Bacterial N uptake:

$$G^C_{BAC,LDON} = G^C_{BAC,LDOC} \times Q^C_{N,LDOM} \quad (\text{A.4.15})$$

$$G^C_{BAC,SDON} = G^C_{BAC,SDOC} \times \min\{ q^C_{N,BAC}, Q^C_{N,SDOM} + fs / N_{f,BAC} \times (q^C_{N,BAC} - Q^C_{N,SDOM}) \} \quad (\text{A.4.16})$$

$$G^C_{BAC,NH4} = G^C_{BAC,LDON} \times NH4 / N_{LDOM} / \min(1, N_{f,BAC}) \quad (\text{A.4.17})$$

if $N_{f,BAC} < 1$,

$$G^C_{BAC,NO3} = \min\{ 0.1 \times NO3 \times 1 / \min(1, N_{f,BAC}) \times (G^C_{BAC,LDON} + G^C_{BAC,SDON}) / (N_{LDOM} + N_{SDOM}), (NO3 + NH4) \times (G^N_{BAC,LDON} + G^N_{BAC,SDON}) / (N_{LDOM} + N_{SDOM}) - G^{NH4}_{BAC} \} \quad (\text{A.4.18})$$

else, $G^C_{BAC,NO3} = 0$ (A.4.19)

$$G^C_{BAC,N} = G^C_{BAC,LDON} + G^C_{BAC,SDON} + G^C_{BAC,NH4} + G^C_{BAC,NO3} \quad (\text{A.4.20})$$

- Bacterial P uptake:



- 750 $G_{BAC,LDOP}^C = G_{BAC,LDOC}^C \times Q_{P,LDOM}^C$ (A.4.21)
- $G_{BAC,SDOP}^C = G_{BAC,SDOC}^C \times \min \{ q_{P,BAC}^C, Q_{P,SDOM}^C + fs/P_{f,BAC} \times (q_{P,BAC}^C - Q_{P,SDOM}^C) \}$ (A.4.22)
- $G_{BAC,PO4}^C = G_{BAC,LDOM}^C \times PO4/P_{LDOM} / \min(1, P_{f,BAC})$ (A.4.23)
- $G_{BAC,P}^C = G_{BAC,LDOP}^C + G_{BAC,SDOP}^C + G_{BAC,PO4}^C$ (A.4.24)
- Respiration:

$$R_{BAC}^C = \zeta^{NO3} \times G_{BAC,NO3}^C + r_{BAC}^B \times T_f \times C_{BAC} + \{ r_{min,BAC}^A + (r_{max,BAC}^A - r_{min,BAC}^A) \times \exp(-br_{BAC} \times G_{BAC,DOC}^C) \} \times G_{BAC,DOC}^C$$
 (A.4.25)
 - RDOC release:

$$E_{BAC,RDOC}^C = refr_{BAC} \times C_{BAC}$$
 (A.4.26)

$$E_{BAC,RDON}^N = E_{BAC,RDOC}^C \times q_{N,RDOM}^C$$
 (A.4.27)

$$E_{BAC,RDOP}^P = E_{BAC,RDOC}^C \times q_{P,RDOM}^C$$
 (A.4.28)
 - Remineralization of inorganic nutrients:

if $Q_{N,BAC}^C > q_{N,BAC}^C$ and $Q_{P,BAC}^C > q_{P,BAC}^C$ (i.e., C in short)

$$REMI_{BAC}^N = remi_{BAC} \times (N_{BAC} - C_{BAC} \times q_{N,BAC}^C)$$
 (A.4.29)

$$REMI_{BAC}^P = remi_{BAC} \times (P_{BAC} - C_{BAC} \times q_{P,BAC}^C)$$
 (A.4.30)

$$remi_{BAC}$$

elseif $Q_{N,BAC}^C < q_{N,BAC}^C$ and $Q_{P,BAC}^C < q_{P,BAC}^C$ (i.e., N in short)

$$REMI_{BAC}^N = 0$$
 (A.4.31)

$$REMI_{BAC}^P = 0$$
 (A.4.32)

else (i.e., P in short)

$$REMI_{BAC}^N = 0$$
 (A.4.33)

$$REMI_{BAC}^P = 0$$
 (A.4.34)
 - SDOM excretion to adjust stoichiometry:

if $Q_{N,BAC}^C > q_{N,BAC}^C$ and $Q_{P,BAC}^C > q_{P,BAC}^C$ (i.e., C in short)

$$E_{BAC,SDOC}^C = 0$$
 (A.4.35)

$$E_{BAC,SDON}^N = 0$$
 (A.4.36)

$$E_{BAC,SDOP}^P = 0$$
 (A.4.37)

elseif $Q_{N,BAC}^C < q_{N,BAC}^C$ and $Q_{P,BAC}^C < q_{P,BAC}^C$ (i.e., N in short)

$$E_{BAC,SDOC}^C = ex_{ADJ,BAC} \times (C_{BAC} - N_{BAC}/q_{N,BAC}^C)$$
 (A.4.38)

$$E_{BAC,SDOC}^N = 0$$
 (A.4.39)

$$E_{BAC,SDOP}^P = ex_{ADJ,BAC} \times (P_{BAC} - N_{BAC}/q_{N,BAC}^C \times q_{P,BAC}^C)$$
 (A.4.40)

else (i.e., P in short)

$$E_{BAC,SDOC}^C = ex_{ADJ,BAC} \times (C_{BAC} - P_{BAC}/q_{P,BAC}^C)$$
 (A.4.41)

$$E_{BAC,SDON}^N = ex_{ADJ,BAC} \times (N_{BAC} - P_{BAC}/q_{P,BAC}^C \times q_{N,BAC}^C)$$
 (A.4.42)

$$E_{BAC,SDOP}^P = 0$$
 (A.4.43)
 - Grazing by microzooplankton:

$$GZ_{BAC}^C = T_f \times \mu_{MZ} \times C_{MZ} \times [C_{BAC}^2 / \{ C_{CR}^2 + g_{BAC}^2 + (C_{DA} \times g_{BAC}/g_{DA})^2 + (C_{CR} \times g_{BAC}/g_{CR})^2 \}]$$
 (A.4.44)

$$GZ_{BAC}^N = GZ_{BAC}^C \times Q_{N,BAC}^C$$
 (A.4.45)

$$GZ_{BAC}^P = GZ_{BAC}^C \times Q_{P,BAC}^C$$
 (A.4.46)
 - Viral mortality:

$$M_{BAC}^C = m_{BAC} \times C_{BAC}$$
 (A.4.47)



- 790 $M_{BAC}^N = m_{BAC} \times N_{BAC}$ (A.4.48)
- $M_{BAC}^P = m_{BAC} \times P_{BAC}$ (A.4.49)
- Net flux of inorganic nutrients through bacteria:
 - $FLUX_{BAC}^{NH4} = REMI_{BAC}^N - G_{BAC,NH4}^C$ (A.4.50)
 - $FLUX_{BAC}^{NO3} = -G_{BAC,NO3}^C$ (A.4.51)
 - $FLUX_{BAC}^{PO4} = REMI_{BAC}^P - G_{BAC,PO4}^C$ (A.4.52)
 - The net growth rate equations:
 - $\frac{dC_{BAC}}{dt} = G_{BAC,DOC}^C - E_{BAC,SDOC}^C - E_{BAC,RDOC}^C - R_{BAC}^C - GZ_{BAC}^C - M_{BAC}^C$ (A.4.53)
 - $\frac{dN_{BAC}}{dt} = G_{BAC,DON}^N - E_{BAC,SDON}^N - E_{BAC,RDON}^N - R_{BAC}^N - GZ_{BAC}^N - M_{BAC}^N$ (A.4.54)
 - $\frac{dP_{BAC}}{dt} = G_{BAC,DOP}^P - E_{BAC,SDOP}^P - E_{BAC,RDOP}^P - R_{BAC}^P - GZ_{BAC}^P - M_{BAC}^P$ (A.4.55)
- 800 **5. Microzooplankton processes**
- Cellular quota (ratio):
 - $Q_{N,MZ}^C = N_{MZ}/C_{MZ}$ (A.5.1)
 - $Q_{P,MZ}^C = C_{MZ}/P_{MZ}$ (A.5.2)
 - Gross growth:
 - $G_{MZ}^C = GZ_{CR}^C + GZ_{BAC}^C$ (A.5.3)
 - $G_{MZ}^N = GZ_{CR}^N + GZ_{BAC}^N$ (A.5.4)
 - $G_{MZ}^P = GZ_{CR}^P + GZ_{BAC}^P$ (A.5.5)
 - LDOM excretion:
 - $E_{MZ,LDOC}^C = f_{ex,MZ} \times ex_{MZ} \times G_{MZ}^C$ (A.5.6)
 - $E_{MZ,LDON}^N = f_{ex,MZ} \times ex_{MZ} \times G_{MZ}^N$ (A.5.7)
 - $E_{MZ,LDOP}^P = f_{ex,MZ} \times ex_{MZ} \times G_{MZ}^P$ (A.5.8)
 - SDOM excretion:
 - $E_{MZ,SDOC,1}^C = (1 - f_{ex,MZ}) \times ex_{MZ} \times G_{MZ}^C$ (A.5.9)
 - $E_{MZ,SDON,1}^N = (1 - f_{ex,MZ}) \times ex_{MZ} \times G_{MZ}^N \times Q_{N,MZ}^C/q_{N,MZ}^C$ (A.5.10)
 - $E_{MZ,SDOP,1}^P = (1 - f_{ex,MZ}) \times ex_{MZ} \times G_{MZ}^P \times Q_{P,MZ}^C/q_{P,MZ}^C$ (A.5.11)
 - SDOM excretion to adjust stoichiometry:
 - $E_{MZ,SDOC,2}^C = ex_{ADJ,MZ} \times C_{MZ} \times \max(0, 1 - Q_{N,MZ}^C/q_{N,MZ}^C, 1 - Q_{P,MZ}^C/q_{P,MZ}^C)$ (A.5.12)
 - $E_{MZ,SDON,2}^N = 0.5 \times E_{MZ,SDOC,2}^C \times Q_{N,MZ}^C$ (A.5.13)
 - $E_{MZ,SDOP,2}^P = 0.5 \times E_{MZ,SDOC,2}^C \times Q_{P,MZ}^C$ (A.5.14)
 - Remineralization of inorganic nutrients:
 - $REMI_{MZ}^N = remi_{MZ} \times \max(0, N_{MZ} - C_{MZ} \times q_{N,MZ}^C, N_{MZ} - q_{N,MZ}^C/P_{MZ} \times q_{P,MZ}^C)$ (A.5.15)
 - $REMI_{MZ}^P = remi_{MZ} \times \max(0, P_{MZ} - C_{MZ} \times q_{P,MZ}^C, P_{MZ} - q_{P,MZ}^C/N_{MZ} \times q_{N,MZ}^C)$ (A.5.16)
 - Respiration:
 - $R_{MZ}^C = r_{MZ}^B \times T_f \times C_{MZ} + r_{MZ}^A \times G_{MZ}^C$ (A.5.17)



- POM production:

$$P_{MZ}^C = pom_{MZ} \times G_{MZ}^C \quad (A.5.18)$$

$$P_{MZ}^N = q_{N,POM}^C \times G_{MZ}^C \quad (A.5.19)$$

$$P_{MZ}^P = q_{P,POM}^C \times G_{MZ}^C \quad (A.5.20)$$

- Grazing by krill:

$$GZ_{MZ}^C = T_f \times \mu_{MZ} \times C_{KR} \times [C_{MZ}^2 / \{ C_{MZ}^2 + g_{MZ}^2 + (C_{DA} \times g_{MZ} / g_{DA})^2 \}] \quad (A.5.21)$$

$$GZ_{MZ}^N = Q_{N,MZ}^C \times GZ_{MZ}^C \quad (A.5.22)$$

$$GZ_{MZ}^P = Q_{P,MZ}^C \times GZ_{MZ}^C \quad (A.5.23)$$

- The net growth rate equations:

$$\frac{dC_{MZ}}{dt} = G_{MZ}^C - E_{MZ,LDOC}^C - E_{MZ,SDOC,1}^C - E_{MZ,SDOC,2}^C - P_{MZ}^C - R_{MZ}^C - GZ_{MZ}^C \quad (A.5.24)$$

$$\frac{dN_{MZ}}{dt} = G_{MZ}^N - E_{MZ,LDON}^N - E_{MZ,SDON,1}^N - E_{MZ,SDON,2}^N - P_{MZ}^N - R_{MZ}^N - GZ_{MZ}^N \quad (A.5.25)$$

$$\frac{dP_{MZ}}{dt} = G_{MZ}^P - E_{MZ,LDOP}^P - E_{MZ,SDOP,1}^P - E_{MZ,SDOP,2}^P - P_{MZ}^P - R_{MZ}^P - GZ_{MZ}^P \quad (A.5.26)$$

6. Krill processes

- Cellular quota (ratio):

$$Q_{N,KR}^C = N_{KR} / C_{KR} \quad (A.6.1)$$

$$Q_{P,KR}^C = C_{KR} / P_{KR} \quad (A.6.2)$$

- Gross growth:

$$G_{KR}^C = GZ_{DA,KR}^C + GZ_{MZ}^C \quad (A.6.3)$$

$$G_{KR}^N = GZ_{DA,KR}^N + GZ_{MZ}^N \quad (A.6.4)$$

$$G_{KR}^P = GZ_{DA,KR}^P + GZ_{MZ}^P \quad (A.6.5)$$

- LDOM excretion:

$$E_{KR,LDOC}^C = f_{ex,KR} \times ex_{KR} \times G_{KR}^C \quad (A.6.6)$$

$$E_{KR,LDON}^N = f_{ex,KR} \times ex_{KR} \times G_{KR}^N \quad (A.6.7)$$

$$E_{KR,LDOP}^P = f_{ex,KR} \times ex_{KR} \times G_{KR}^P \quad (A.6.8)$$

- SDOM excretion:

$$E_{KR,SDOC,1}^C = (1 - f_{ex,KR}) \times ex_{KR} \times G_{KR}^C \quad (A.6.9)$$

$$E_{KR,SDON,1}^N = (1 - f_{ex,KR}) \times ex_{KR} \times G_{KR}^N \times Q_{N,KR}^C / q_{N,KR}^C \quad (A.6.10)$$

$$E_{KR,SDOP,1}^P = (1 - f_{ex,KR}) \times ex_{KR} \times G_{KR}^P \times Q_{P,KR}^C / q_{P,KR}^C \quad (A.6.11)$$

- SDOM excretion to adjust stoichiometry:

$$E_{KR,SDOC,2}^C = ex_{ADJ,KR} \times C_{KR} \times \max(0, 1 - Q_{N,KR}^C / q_{N,KR}^C, 1 - Q_{P,KR}^C / q_{P,KR}^C) \quad (A.6.12)$$

$$E_{KR,SDON,2}^N = 0.5 \times E_{KR,SDOC,2}^C \times Q_{N,KR}^C \quad (A.6.13)$$

$$E_{KR,SDOP,2}^P = 0.5 \times E_{KR,SDOC,2}^C \times Q_{P,KR}^C \quad (A.6.14)$$

- Remineralization of inorganic nutrients:



$$REMI_{KR}^N = remi_{KR} \times \max(0, N_{KR} - C_{KR} \times q_{N,KR}^C, N_{KR} - q_{N,KR}^C / P_{KR} \times q_{P,KR}^C) \quad (A.6.15)$$

$$REMI_{KR}^P = remi_{KR} \times \max(0, P_{KR} - C_{KR} \times q_{P,KR}^C, P_{KR} - q_{P,KR}^C / N_{KR} \times q_{N,KR}^C) \quad (A.6.16)$$

870

- Respiration:

$$R_{KR}^C = r_{KR}^B \times T_f \times C_{KR} + r_{KR}^A \times G_{KR}^C \quad (A.6.17)$$

- POM production:

$$P_{KR}^C = pom_{KR} \times G_{KR}^C \quad (A.6.18)$$

875

$$P_{KR}^N = q_{N,POM}^C \times G_{KR}^N \quad (A.6.19)$$

$$P_{KR}^P = q_{P,POM}^C \times G_{KR}^P \quad (A.6.20)$$

- RDOC release:

$$E_{KR,RDOC}^C = refr_{KR} \times C_{KR} \quad (A.6.21)$$

$$E_{KR,RDON}^N = E_{KR,RDOC}^C \times q_{N,RDOM}^C \quad (A.6.22)$$

880

$$E_{KR,RDOP}^P = E_{KR,RDOC}^C \times q_{P,RDOM}^C \quad (A.6.23)$$

- Removal by higher trophic levels

$$M_{KR}^C = mort_{KR} \times C_{KR} \times C_{KR} \quad (A.6.24)$$

$$M_{KR}^N = M_{KR,RDOC}^C \times Q_{N,KR}^C \quad (A.6.25)$$

$$M_{KR}^P = M_{KR,RDOC}^C \times Q_{P,KR}^C \quad (A.6.26)$$

885

- The net growth rate equations:

$$\frac{dC_{KR}}{dt} = G_{KR}^C - E_{KR,LDOC}^C - E_{KR,SDOC,1}^C - E_{KR,SDOC,2}^C - E_{KR,RDOC}^C - P_{KR}^C - R_{KR}^C - M_{KR}^C \quad (A.6.27)$$

$$\frac{dN_{KR}}{dt} = G_{KR}^N - E_{KR,LDON}^N - E_{KR,SDON,1}^N - E_{KR,SDON,2}^N - E_{KR,RDON}^N - P_{KR}^N - R_{KR}^N - M_{KR}^N \quad (A.6.28)$$

890

$$\frac{dP_{KR}}{dt} = G_{KR}^P - E_{KR,LDOC}^P - E_{KR,SDOC,1}^P - E_{KR,SDOC,2}^P - E_{KR,RDOC}^P - P_{KR}^P - R_{KR}^P - M_{KR}^P \quad (A.6.29)$$

7. Detrital processes

- Dissolution:

$$DISS_{DET}^C = diss \times C_{DET} \quad (A.7.1)$$

$$DISS_{DET}^N = diss \times prf_N \times N_{DET} \quad (A.7.2)$$

$$DISS_{DET}^P = diss \times prf_P \times P_{DET} \quad (A.7.3)$$

- The net change equations:

$$\frac{dC_{DET}}{dt} = D_{DA}^C + D_{CR}^C + D_{MZ}^C + D_{KR}^C + DISS_{HZ}^C - DISS_{DET}^C \quad (A.7.4)$$

900

$$\frac{dN_{DET}}{dt} = D_{DA}^N + D_{CR}^N + D_{MZ}^N + D_{KR}^N + DISS_{HZ}^N - DISS_{DET}^N \quad (A.7.5)$$

$$\frac{dP_{DET}}{dt} = D_{DA}^P + D_{CR}^P + D_{MZ}^P + D_{KR}^P + DISS_{HZ}^P - DISS_{DET}^P \quad (A.7.6)$$

where $DISS_{HZ}^C = f_{POM,HZ} \times M_{KR}^C$



$$DISS^N_{HZ} = f_{POM,HZ} \times M^N_{KR}$$

$$DISS^P_{HZ} = f_{POM,HZ} \times M^P_{KR}$$

905

8. DOM processes

- Conversion of SDOM to RDOM:

$$REFR^C_{SDOM} = exREFR_{SDOM} \times C_{SDOM} \times \exp\{1 - \min(Q^C_{N,SDOM}/q^C_{N,RDOM}, Q^C_{P,SDOM}/q^C_{P,RDOM})\} \quad (A.8.1)$$

$$REFR^N_{SDOM} = REFR^C_{SDOM} \times q^C_{N,RDOM} \quad (A.8.2)$$

$$REFR^P_{SDOM} = REFR^C_{SDOM} \times q^C_{P,RDOM} \quad (A.8.3)$$

910

- The net change equations:

$$\frac{dC_{LDOM}}{dt} = E^C_{DA,LDOC} + E^C_{CR,LDOC} + E^C_{MZ,LDOC} + E^C_{KR,LDOC} + M^C_{BAC} - G^C_{BAC,LDOC} \quad (A.8.4)$$

$$\frac{dN_{LDOM}}{dt} = E^N_{DA,LDON} + E^N_{CR,LDON} + E^N_{MZ,LDON} + E^N_{KR,LDON} + M^N_{BAC} - G^N_{BAC,LDON} \quad (A.8.5)$$

$$\frac{dP_{LDOM}}{dt} = E^P_{DA,LDOP} + E^P_{CR,LDOP} + E^P_{MZ,LDOP} + E^P_{KR,LDOP} + M^P_{BAC} - G^P_{BAC,LDOP} \quad (A.8.6)$$

915

$$\begin{aligned} \frac{dC_{SDOM}}{dt} = & E^C_{DA,SDOC} + E^C_{CR,SDOC} + E^C_{BAC,SDOC} + E^C_{MZ,SDOC,1} + E^C_{MZ,SDOC,2} \\ & + E^C_{KR,SDOC,1} + E^C_{KR,SDOC,2} + E^C_{HZ,SDOC} + DISS^C_{DET} - REFR^C_{SDOM} - G^C_{BAC,SDOC} \end{aligned} \quad (A.8.7)$$

$$\begin{aligned} \frac{dN_{SDOM}}{dt} = & E^N_{DA,SDON} + E^N_{CR,SDON} + E^N_{BAC,SDON} + E^N_{MZ,SDON,1} + E^N_{MZ,SDON,2} \\ & + E^N_{KR,SDON,1} + E^N_{KR,SDON,2} + E^N_{HZ,SDON} + DISS^N_{DET} - REFR^N_{SDOM} - G^N_{BAC,SDON} \end{aligned} \quad (A.8.8)$$

$$\begin{aligned} \frac{dP_{SDOM}}{dt} = & E^P_{DA,SDOP} + E^P_{CR,SDOP} + E^P_{BAC,SDOP} + E^P_{MZ,SDOP,1} + E^P_{MZ,SDOP,2} \\ & + E^P_{KR,SDOP,1} + E^P_{KR,SDOP,2} + E^P_{HZ,SDOP} + DISS^P_{DET} - REFR^P_{SDOM} - G^P_{BAC,SDOP} \end{aligned} \quad (A.8.9)$$

920

9. Dissolved inorganic nutrient processes

- Nitrification:

$$NTRF = r_{nrf} \times NH4 \quad (A.9.1)$$

925

- The net change equations:

$$\frac{dNH4}{dt} = FLUX^{NH4}_{BAC} + REMI^N_{MZ} + REMI^N_{KR} + REMI^N_{HZ} - G^{NH4}_{DA} - G^{NH4}_{CR} - NTRF \quad (A.9.2)$$

$$\frac{dNO3}{dt} = FLUX^{NO3}_{BAC} - G^{NO3}_{DA} - G^{NO3}_{CR} + NTRF \quad (A.9.3)$$

$$\frac{dPO4}{dt} = FLUX^{PO4}_{BAC} + REMI^P_{MZ} + REMI^P_{KR} + REMI^P_{HZ} - G^{PO4}_{DA} - G^{PO4}_{CR} \quad (A.9.4)$$

$$\text{where } REMI^N_{HZ} = M^N_{KR} - D^N_{HZ} - E^{SDON}_{HZ}$$

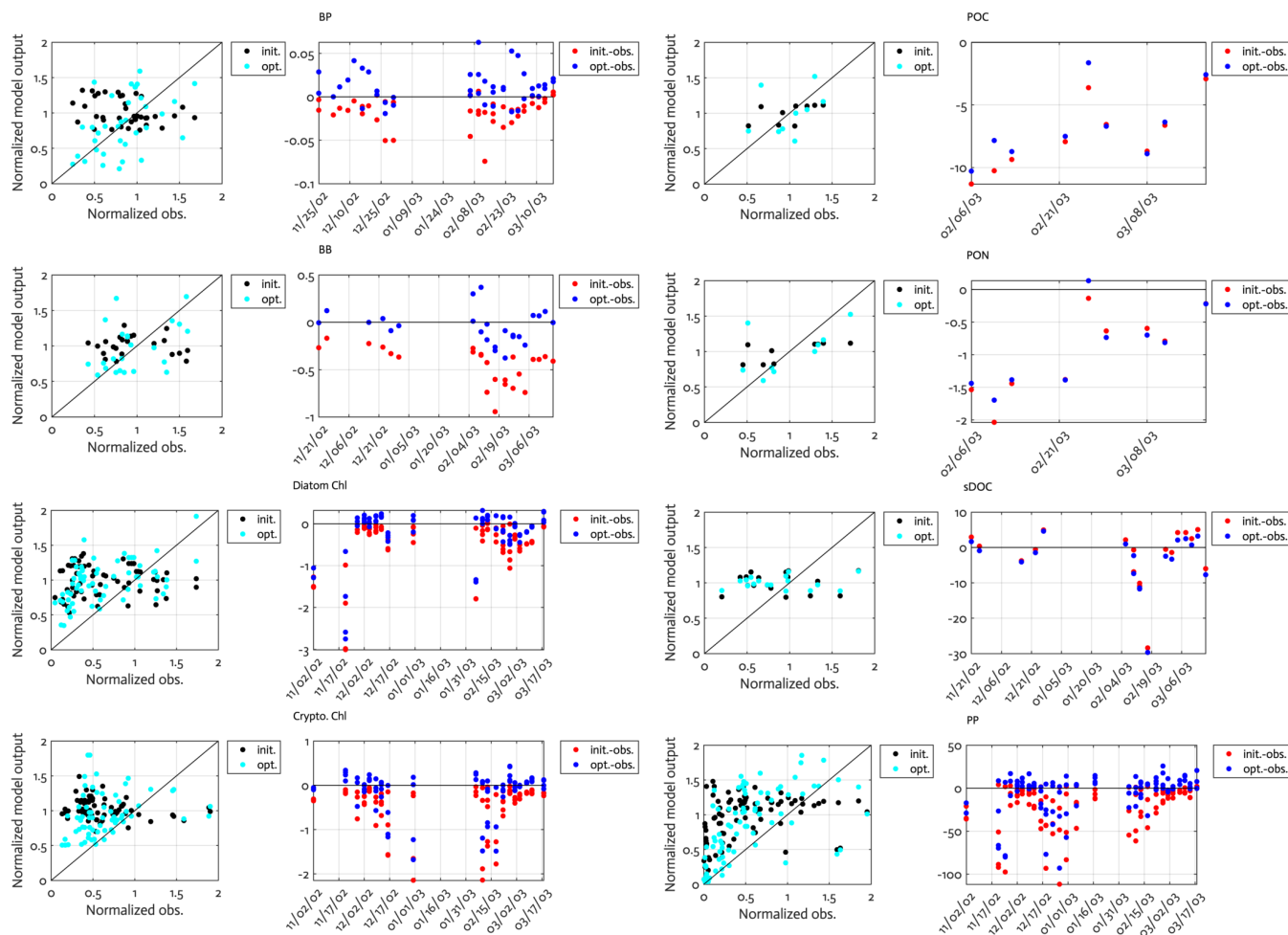
$$REMI^P_{HZ} = M^P_{KR} - D^P_{HZ} - E^{SDOP}_{HZ}$$

930



Appendix B

935 **Figure B1.** Comparison of the observations to model results from initial guess values and optimized model parameters. Errors represent how much larger model output is compared to observations. Normalized observation: observations normalized by the mean of each model state variable.



940



Figure B2. The errors (standard deviation) of the model state variables for the modelled growth season (x-axis; month/day) from the Monte Carlo experiments ($N = 1,000$). Note different contour scales among panels.

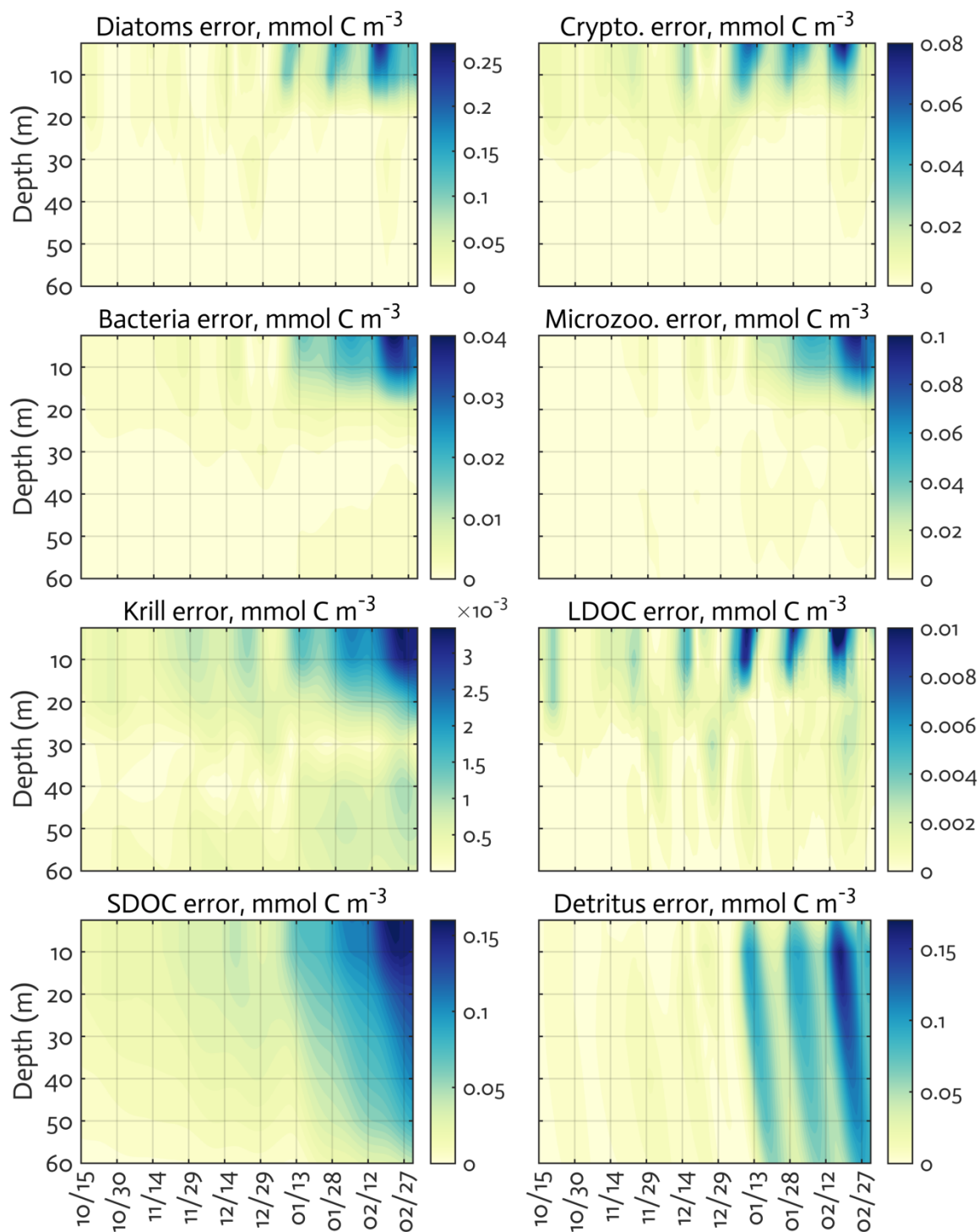




Figure B3. The model state variables for the modelled growth season (x-axis; month/day) using the initial parameter guess values (i.e., before optimization). Note different contour scales among panels.

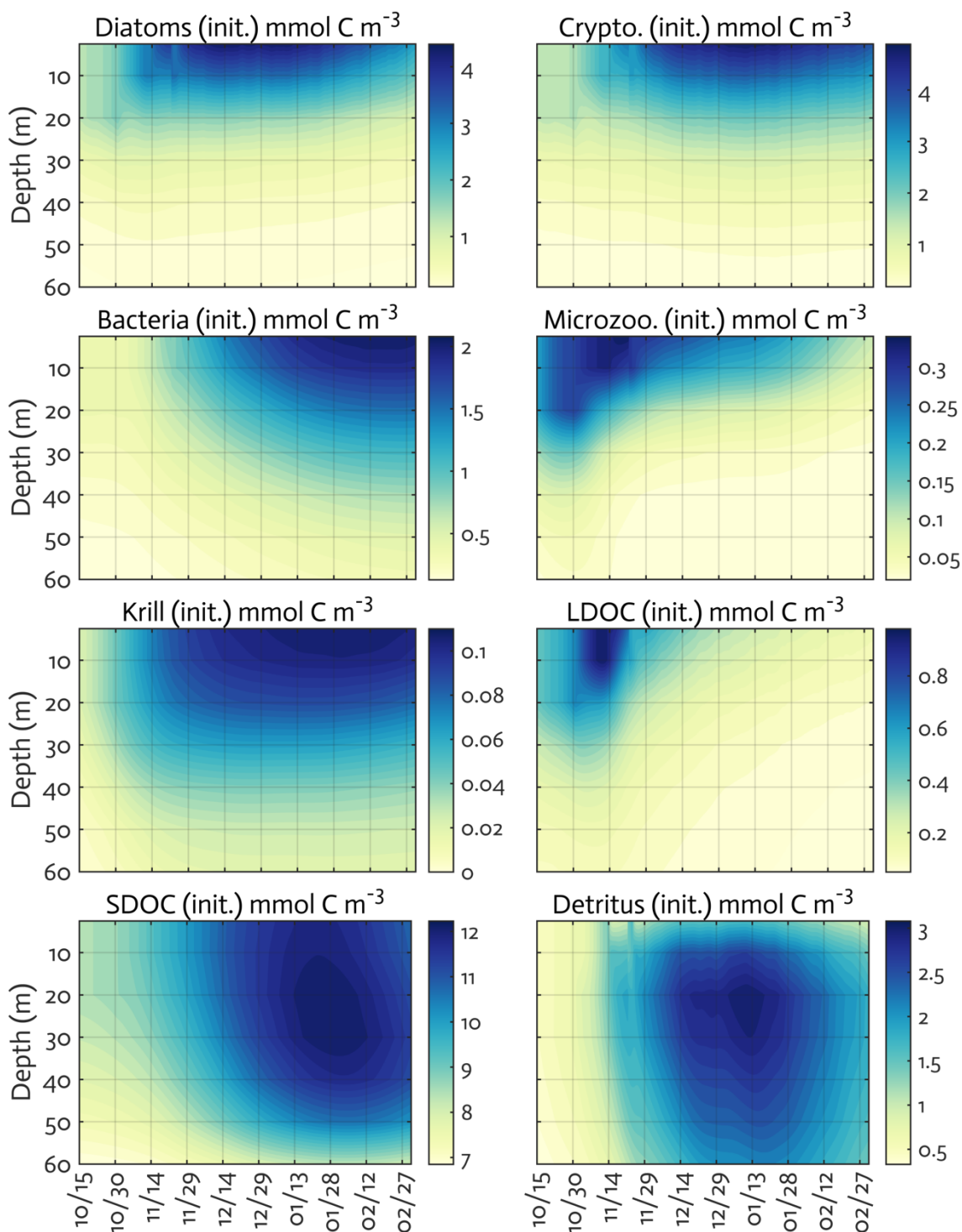
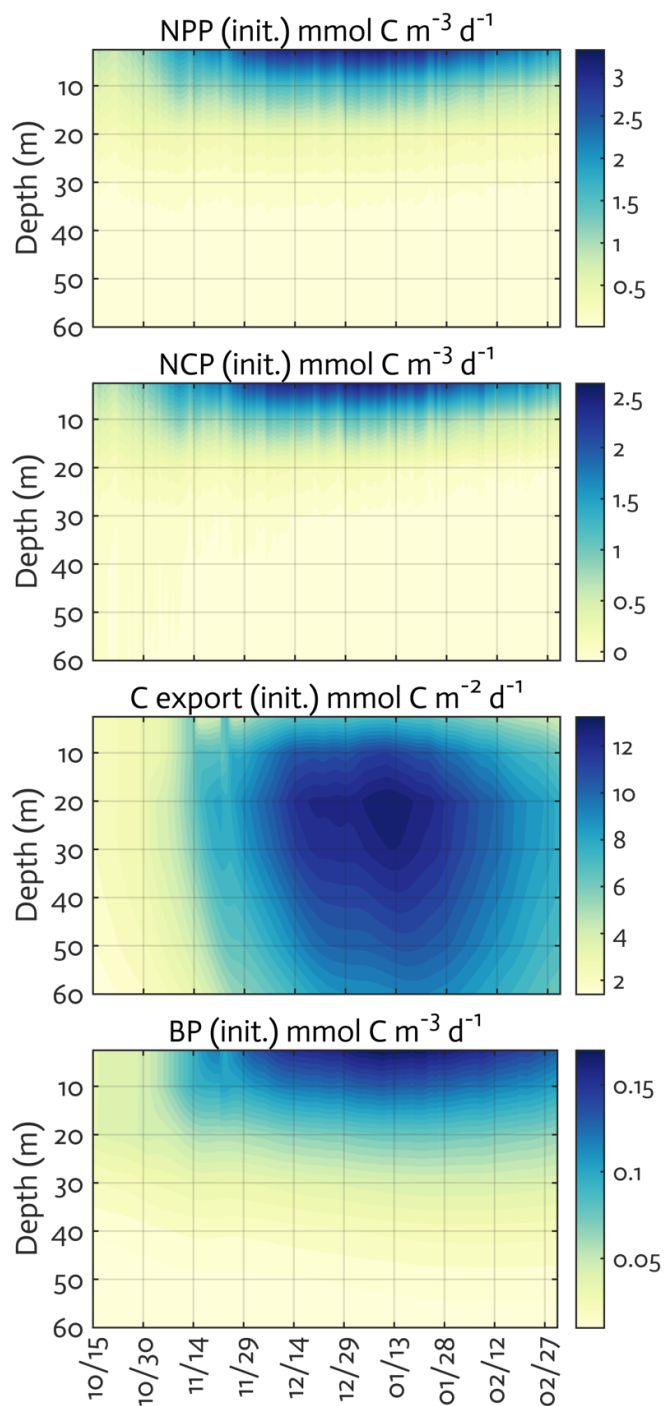


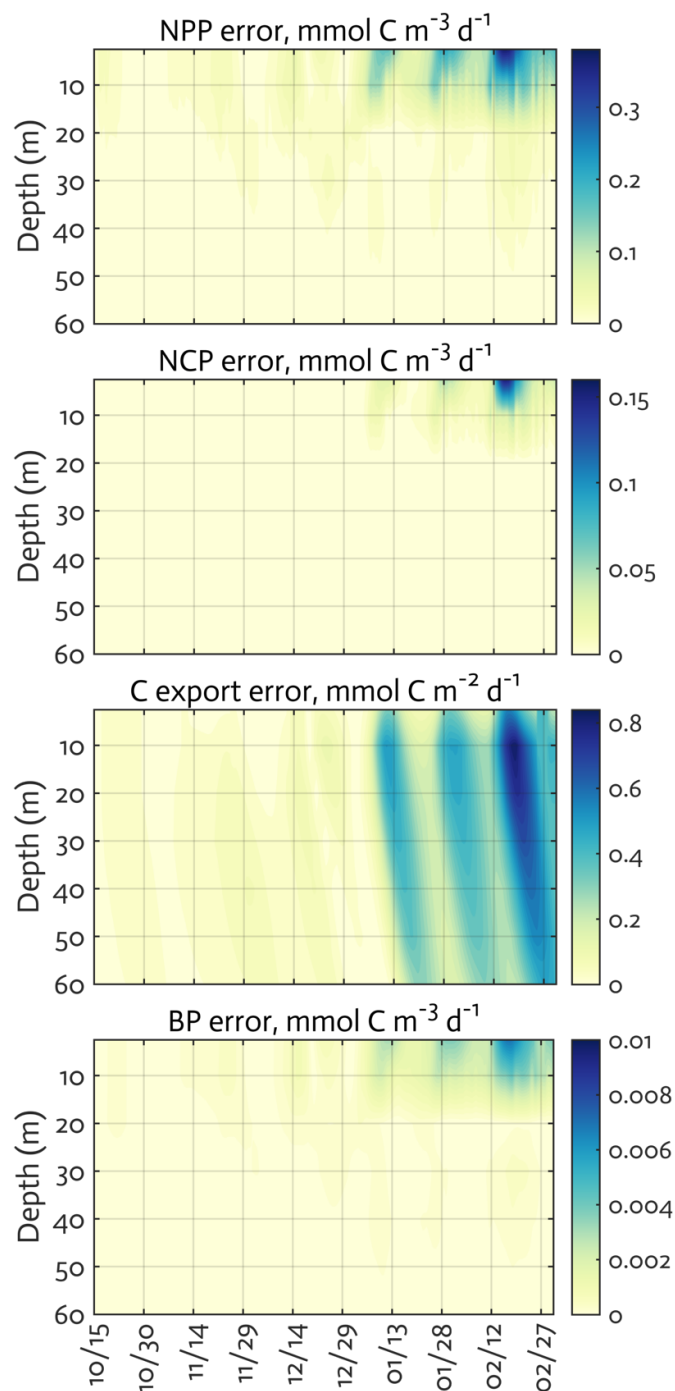


Figure B4. The ecosystem indices for the modelled growth season (x-axis; month/day) using the initial parameter guess values (i.e., before optimization). Note different contour scales among panels.





955 **Figure B5.** The errors (standard deviation) of the ecosystem indices for the modelled growth season (x-axis; month/day) from the Monte Carlo experiments ($N = 1,000$). Note different contour scales among panels.





960 References

- Bertilsson, S., Berglund, O., Karl, D. M., & Chisholm, S. W. (2003). Elemental composition of marine Prochlorococcus and Synechococcus: Implications for the ecological stoichiometry of the sea. *Limnology and Oceanography*, 48(5), 1721–1731. <https://doi.org/10.4319/lo.2003.48.5.1721>
- 965 Bird, D. F., & Karl, D. M. (1999). Uncoupling of bacteria and phytoplankton during the austral spring bloom in Gerlache Strait, Antarctic Peninsula. *Aquatic Microbial Ecology*, 19(1), 13–27. <https://doi.org/10.3354/ame019013>
- Bowman, J. S., & Ducklow, H. W. (2015). Microbial Communities Can Be Described by Metabolic Structure: A General Framework and Application to a Seasonally Variable, Depth-Stratified Microbial Community from the Coastal West Antarctic Peninsula. *PLOS ONE*, 10(8), e0135868. <https://doi.org/10.1371/journal.pone.0135868>
- 970 Bowman, J. S., Kavanaugh, M. T., Doney, S. C., & Ducklow, H. W. (2018). Recurrent seascape units identify key ecological processes along the western Antarctic Peninsula. *Global Change Biology*, 24(7), 3065–3078. <https://doi.org/10.1111/gcb.14161>
- Campbell, J. W. (1995). The lognormal distribution as a model for bio-optical variability in the sea. *Journal of Geophysical Research: Oceans*, 100(C7), 13237–13254. <https://doi.org/10.1029/95JC00458>
- 975 Carlson, C. A., Bates, N. R., Ducklow, H. W., & Hansell, D. A. (1999). Estimation of bacterial respiration and growth efficiency in the Ross Sea, Antarctica. *Aquatic Microbial Ecology*, 19(3), 229–244.
- Clarke, A., Griffiths, H. J., Barnes, D. K. A., Meredith, M. P., & Grant, S. M. (2009). Spatial variation in seabed temperatures in the Southern Ocean: Implications for benthic ecology and biogeography. *Journal of Geophysical Research: Biogeosciences*, 114(G3). <https://doi.org/10.1029/2008JG000886>
- 980 Cook, A. J., Fox, A. J., Vaughan, D. G., & Ferrigno, J. G. (2005). Retreating Glacier Fronts on the Antarctic Peninsula over the Past Half-Century. *Science*, 308(5721), 541–544. <https://doi.org/10.1126/science.1104235>
- del Giorgio, P. A., & Cole, J. J. (1998). Bacterial Growth Efficiency in Natural Aquatic Systems. *Annual Review of Ecology and Systematics*, 29(1), 503–541. <https://doi.org/10.1146/annurev.ecolsys.29.1.503>
- 985 Doney, S. C., Glover, D. M., McCue, S. J., & Fuentes, M. (2003). Mesoscale variability of Sea-viewing Wide Field-of-view Sensor (SeaWiFS) satellite ocean color: Global patterns and spatial scales. *Journal of Geophysical Research: Oceans*, 108(C2). <https://doi.org/10.1029/2001JC000843>
- Doney, S. C., Lima, I., Moore, J. K., Lindsay, K., Behrenfeld, M. J., Westberry, T. K., Mahowald, N., Glover, D. M., & Takahashi, T. (2009). Skill metrics for confronting global upper ocean ecosystem-biogeochemistry models against field and remote sensing data. *Journal of Marine Systems*, 76(1), 95–112. <https://doi.org/10.1016/j.jmarsys.2008.05.015>
- 990 Droop, M. R. (1974). The nutrient status of algal cells in continuous culture. *Journal of the Marine Biological Association of the United Kingdom*, 54(4), 825–855. <https://doi.org/10.1017/S002531540005760X>
- Droop, M. R. (1983). 25 years of algal growth kinetics. A personal view. *Botanica Marina*. <http://agris.fao.org/agris-search/search.do?recordID=US201302597810>
- 995 Ducklow, H. W. (2000). Bacterial production and biomass in the ocean. In *Microbial Ecology of the Oceans, Second Edition* (pp. 85–120). John Wiley & Sons, Inc.
- Ducklow, H. W., Doney, S. C., & Steinberg, D. K. (2008). Contributions of Long-Term Research and Time-Series Observations to Marine Ecology and Biogeochemistry. *Annual Review of Marine Science*, 1, 279–302.
- Ducklow, Hugh W, Baker, K., Martinson, D. G., Quetin, L. B., Ross, R. M., Smith, R. C., Stammerjohn, S. E., Vernet, M., & Fraser, W. (2007). Marine pelagic ecosystems: The West Antarctic Peninsula. *Philosophical Transactions of the Royal Society B: Biological Sciences*, 362(1477), 67–94. <https://doi.org/10.1098/rstb.2006.1955>
- 1000 Ducklow, Hugh W., & Doney, S. C. (2013). What is the metabolic state of the oligotrophic ocean? A debate. *Annual Review of Marine Science*, 5, 525–533. <https://doi.org/10.1146/annurev-marine-121211-172331>
- Ducklow, Hugh W., Myers, K. M. S., Erickson, M., Ghiglione, J.-F., & Murray, A. E. (2011). *Response of a summertime Antarctic marine-bacterial community to glucose and ammonium enrichment*. <http://agris.fao.org/agris-search/search.do?recordID=AV2012072112>
- 1005 Ducklow, Hugh W., Schofield, O., Vernet, M., Stammerjohn, S., & Erickson, M. (2012). Multiscale control of bacterial production by phytoplankton dynamics and sea ice along the western Antarctic Peninsula: A regional and decadal investigation. *Journal of Marine Systems*, 98–99, 26–39. <https://doi.org/10.1016/j.jmarsys.2012.03.003>



- 1010 Ducklow, Hugh W., Stukel, M. R., Eveleth, R., Doney, S. C., Jickells, T., Schofield, O., Baker, A. R., Brindle, J., Chance, R., & Cassar, N. (2018). Spring–summer net community production, new production, particle export and related water column biogeochemical processes in the marginal sea ice zone of the Western Antarctic Peninsula 2012–2014. *Philosophical Transactions of the Royal Society A: Mathematical, Physical and Engineering Sciences*, 376(2122), 20170177. <https://doi.org/10.1098/rsta.2017.0177>
- 1015 Dugdale, R. C., & Goering, J. J. (1967). Uptake of New and Regenerated Forms of Nitrogen in Primary Productivity. *Limnology and Oceanography*, 12(2), 196–206. <https://doi.org/10.4319/lo.1967.12.2.0196>
- Fennel, K., Losch, M., Schröter, J., & Wenzel, M. (2001). Testing a marine ecosystem model: Sensitivity analysis and parameter optimization. *Journal of Marine Systems*, 28(1), 45–63. [https://doi.org/10.1016/S0924-7963\(00\)00083-X](https://doi.org/10.1016/S0924-7963(00)00083-X)
- Friedrichs, M. A. M. (2001). Assimilation of JGOFS EqPac and SeaWiFS data into a marine ecosystem model of the Central Equatorial Pacific Ocean. *Deep Sea Research Part II: Topical Studies in Oceanography*, 49(1), 289–319.
- 1020 Friedrichs, M. A. M., Dusenberry, J. A., Anderson, L. A., Armstrong, R. A., Chai, F., Christian, J. R., Doney, S. C., Dunne, J., Fujii, M., Hood, R., McGillicuddy, D. J., Moore, J. K., Schartau, M., Spitz, Y. H., & Wiggert, J. D. (2007). Assessment of skill and portability in regional marine biogeochemical models: Role of multiple planktonic groups. *Journal of Geophysical Research: Oceans*, 112(C8).
- 1025 Friedrichs, M. A. M., Hood, R. R., & Wiggert, J. D. (2006). Ecosystem model complexity versus physical forcing: Quantification of their relative impact with assimilated Arabian Sea data. *Deep Sea Research Part II: Topical Studies in Oceanography*, 53(5), 576–600.
- Fukuda, R., Ogawa, H., Nagata, T., & Koike, I. (1998). Direct Determination of Carbon and Nitrogen Contents of Natural Bacterial Assemblages in Marine Environments. *Applied and Environmental Microbiology*, 64(9), 3352–3358.
- 1030 Garzio, L. M., Steinberg, D. K., Erickson, M., & Ducklow, H. W. (2013). Microzooplankton grazing along the Western Antarctic Peninsula. <https://doi.org/10.3354/ame01655>
- Garzio, L., & Steinberg, D. (2013). Microzooplankton community composition along the Western Antarctic Peninsula. *Deep Sea Research Part I: Oceanographic Research Papers*, 77, 36–49. <https://doi.org/10.1016/j.dsr.2013.03.001>
- 1035 Geider, R. J., MacIntyre, H. L., & Kana, T. M. (1997). Dynamic model of phytoplankton growth and acclimation: Responses of the balanced growth rate and the chlorophyll a: carbon ratio to light, nutrient-limitation and temperature. *Marine Ecology Progress Series*, 148(1/3), 187–200. JSTOR.
- Geider, Richard J. (1987). Light and Temperature Dependence of the Carbon to Chlorophyll a Ratio in Microalgae and Cyanobacteria: Implications for Physiology and Growth of Phytoplankton. *The New Phytologist*, 106(1), 1–34. JSTOR.
- 1040 Gilbert, J. C., & Lemaréchal, C. (1989). Some numerical experiments with variable-storage quasi-Newton algorithms. *Mathematical Programming*, 45(1), 407–435.
- Glover, D. M., Doney, S. C., Oestreich, W. K., & Tullo, A. W. (2018). Geostatistical Analysis of Mesoscale Spatial Variability and Error in SeaWiFS and MODIS/Aqua Global Ocean Color Data. *Journal of Geophysical Research: Oceans*, 123(1), 22–39. <https://doi.org/10.1002/2017JC013023>
- 1045 Glover, D. M., Jenkins, W. J., & Doney, S. C. (2011). 10. Model analysis and optimization. In *Modeling Methods for Marine Science*. Cambridge University Press.
- Harmon, R., & Challenor, P. (1997). A Markov chain Monte Carlo method for estimation and assimilation into models. *Ecological Modelling*, 101(1), 41–59. [https://doi.org/10.1016/S0304-3800\(97\)01947-9](https://doi.org/10.1016/S0304-3800(97)01947-9)
- 1050 Henley, S. F., Schofield, O. M., Hendry, K. R., Schloss, I. R., Steinberg, D. K., Moffat, C., Peck, L. S., Costa, D. P., Bakker, D. C. E., Hughes, C., Rozema, P. D., Ducklow, H. W., Abele, D., Stefels, J., Van Leeuwe, M. A., Brussaard, C. P. D., Buma, A. G. J., Kohut, J., Sahade, R., ... Meredith, M. P. (2019). Variability and change in the west Antarctic Peninsula marine system: Research priorities and opportunities. *Progress in Oceanography*, 173, 208–237. <https://doi.org/10.1016/j.pocean.2019.03.003>
- 1055 Kim, H., Doney, S. C., Iannuzzi, R. A., Meredith, M. P., Martinson, D. G., & Ducklow, H. W. (2016). Climate forcing for dynamics of dissolved inorganic nutrients at Palmer Station, Antarctica: An interdecadal (1993–2013) analysis. *Journal of Geophysical Research: Biogeosciences*, 121(9), 2369–2389.
- Kim, H., & Ducklow, H. W. (2016). A decadal (2002–2014) analysis for dynamics of heterotrophic bacteria in an Antarctic coastal ecosystem: Variability and physical and biogeochemical Forcings. *Frontiers in Marine Science*, 3. <https://doi.org/10.3389/fmars.2016.00214>



- 1060 King, J. C. (1994). Recent climate variability in the vicinity of the antarctic peninsula. *International Journal of Climatology*, 14(4), 357–369. <https://doi.org/10.1002/joc.3370140402>
- Kirchman, D. L., Morán, X. A. G., & Ducklow, H. (2009). Microbial growth in the polar oceans—Role of temperature and potential impact of climate change. *Nature Reviews Microbiology*, 7(6), 451–459.
- Klinck, J. M. (1998). Heat and salt changes on the continental shelf west of the Antarctic Peninsula between January 1993 and January 1994. *Journal of Geophysical Research: Oceans*, 103(C4), 7617–7636.
1065 <https://doi.org/10.1029/98JC00369>
- Lawson, L. M., Spitz, Y. H., Hofmann, E. E., & Long, R. B. (1995). A data assimilation technique applied to a predator-prey model. *Bulletin of Mathematical Biology*, 57(4), 593–617.
- Legendre, L., & Rassoulzadegan, F. (1996). Food-web mediated export of biogenic carbon in oceans: hydrodynamic control. *Marine Ecology Progress Series*, 145, 179–193. <https://doi.org/10.3354/meps145179>
- 1070 Luo, Y.-W., Friedrichs, M. A. M., Doney, S. C., Church, M. J., & Ducklow, H. W. (2010). Oceanic heterotrophic bacterial nutrition by semilabile DOM as revealed by data assimilative modeling. *Aquatic Microbial Ecology*, 60(3), 273–287.
- Luria, C. M., Amaral-Zettler, L. A., Ducklow, H. W., Repeta, D. J., Rhyne, A. L., & Rich, J. J. (2017). Seasonal Shifts in Bacterial Community Responses to Phytoplankton-Derived Dissolved Organic Matter in the Western Antarctic Peninsula. *Frontiers in Microbiology*, 8. <https://doi.org/10.3389/fmicb.2017.02117>
- 1075 Luria, C. M., Ducklow, H. W., & Amaral-Zettler, L. A. (2014). *Marine bacterial, archaeal and eukaryotic diversity and community structure on the continental shelf of the western Antarctic Peninsula*. <https://doi.org/10.3354/ame01703>
- Matear, R. J. (1996). Parameter optimization and analysis of ecosystem models using simulated annealing: A case study at Station P. *Oceanographic Literature Review*, 43(6). <https://doi.org/info:doi/10.1357/0022240953213098>
- 1080 McCarthy, J. (1980). *Nitrogen*. In: *Morris I (ed) The physiological ecology of phytoplankton*. Blackwell, Oxford.
- Meredith, M. P., & King, J. C. (2005). Rapid climate change in the ocean west of the Antarctic Peninsula during the second half of the 20th century. *Geophysical Research Letters*, 32(19). <https://doi.org/10.1029/2005GL024042>
- Moline, M., Karnovsky, N., Brown, Z., Divoky, G., Frazer, T., Jacoby, C., Torres, J., & Fraser, W. (2008). High Latitude Changes in Ice Dynamics and Their Impact on Polar Marine Ecosystems. *Annals of the New York Academy of Sciences*, 1134, 267–319. <https://doi.org/10.1196/annals.1439.010>
- 1085 Montégut, C. de B., Madec, G., Fischer, A. S., Lazar, A., & Iudicone, D. (2004). Mixed layer depth over the global ocean: An examination of profile data and a profile-based climatology. *Journal of Geophysical Research: Oceans*, 109(C12). <https://doi.org/10.1029/2004JC002378>
- Montes-Hugo, M., Doney, S. C., Ducklow, H. W., Fraser, W., Martinson, D., Stammerjohn, S. E., & Schofield, O. (2009). Recent Changes in Phytoplankton Communities Associated with Rapid Regional Climate Change Along the Western Antarctic Peninsula. *Science*, 323(5920), 1470–1473. <https://doi.org/10.1126/science.1164533>
- 1090 Murphy, E. J., Cavanagh, R. D., Hofmann, E. E., Hill, S. L., Constable, A. J., Costa, D. P., Pinkerton, M. H., Johnston, N. M., Trathan, P. N., Klinck, J. M., Wolf-Gladrow, D. A., Daly, K. L., Maury, O., & Doney, S. C. (2012). Developing integrated models of Southern Ocean food webs: Including ecological complexity, accounting for uncertainty and the importance of scale. *Progress in Oceanography*, 102, 74–92. [https://doi.org/Murphy, E.J](https://doi.org/Murphy,E.J) ORCID: <https://orcid.org/0000-0002-7369-9196> <<https://orcid.org/0000-0002-7369-9196>>; Cavanagh, R.D. ORCID: <https://orcid.org/0000-0002-2474-9716> <<https://orcid.org/0000-0002-2474-9716>>; Hofmann, E.E.; Hill, S.L.; Constable, A.J.; Costa, D.P.; Pinkerton, M.H.; Johnston, N.M.; Trathan, P.N.; Klinck, J.M.; Wolf-Gladrow, D.A.; Daly, K.L.; Maury, O.; Doney, S.C.. 2012 Developing integrated models of Southern Ocean food webs: including ecological complexity, accounting for uncertainty and the importance of scale. *Progress in Oceanography*, 102, 74–92. <https://doi.org/10.1016/j.pocean.2012.03.006> <<https://doi.org/10.1016/j.pocean.2012.03.006>>
- 1095
- 1100 Pomeroy, L. R., & Wiebe, W. J. (2001). Temperature and substrates as interactive limiting factors for marine heterotrophic bacteria. *Aquatic Microbial Ecology*, 23(2), 187–204. <https://doi.org/10.3354/ame023187>
- 1105 Prunet, P., Minster, J.-F., Echevin, V., & Dadou, I. (1996). Assimilation of surface data in a one-dimensional physical-biogeochemical model of the surface ocean: 2. Adjusting a simple trophic model to chlorophyll, temperature, nitrate, and pCO₂ data. *Global Biogeochemical Cycles*, 10(1), 139–158. <https://doi.org/10.1029/95GB03435>



- Prunet, P., Minster, J.-F., Ruiz-Pino, D., & Dadou, I. (1996). Assimilation of surface data in a one-dimensional physical-biogeochemical model of the surface ocean: 1. Method and preliminary results. *Global Biogeochemical Cycles*, 10(1), 111–138. <https://doi.org/10.1029/95GB03436>
- 1110 Saba, G. K., Fraser, W. R., Saba, V. S., Iannuzzi, R. A., Coleman, K. E., Doney, S. C., Ducklow, H. W., Martinson, D. G., Miles, T. N., Patterson-Fraser, D. L., Stammerjohn, S. E., Steinberg, D. K., & Schofield, O. M. (2014). Winter and spring controls on the summer food web of the coastal West Antarctic Peninsula. *Nature Communications*, 5(1), 1–8. <https://doi.org/10.1038/ncomms5318>
- 1115 Saille, S. F., Ducklow, H. W., Moeller, H. V., Fraser, W. R., Schofield, O. M., Steinberg, D. K., Garzio, L. M., & Doney, S. C. (2013). Carbon fluxes and pelagic ecosystem dynamics near two western Antarctic Peninsula Adélie penguin colonies: An inverse model approach. *Marine Ecology Progress Series*, 492, 253–272. <https://doi.org/10.3354/meps10534>
- 1120 Schofield, O., Saba, G., Coleman, K., Carvalho, F., Couto, N., Ducklow, H., Finkel, Z., Irwin, A., Kahl, A., Miles, T., Montes-Hugo, M., Stammerjohn, S., & Waite, N. (2017). Decadal variability in coastal phytoplankton community composition in a changing West Antarctic Peninsula. *Deep Sea Research Part I: Oceanographic Research Papers*, 124, 42–54. <https://doi.org/10.1016/j.dsr.2017.04.014>
- Sherrell, R. M., Annett, A. L., Fitzsimmons, J. N., Rocanova, V. J., & Meredith, M. P. (2018). A “shallow bathtub ring” of local sedimentary iron input maintains the Palmer Deep biological hotspot on the West Antarctic Peninsula shelf. *Philosophical Transactions. Series A, Mathematical, Physical, and Engineering Sciences*, 376(2122). <https://doi.org/10.1098/rsta.2017.0171>
- 1125 Smith, D. A., Hofmann, E. E., Klinck, J. M., & Lascara, C. M. (1999). Hydrography and circulation of the West Antarctic Peninsula Continental Shelf. *Deep Sea Research Part I: Oceanographic Research Papers*, 46(6), 925–949. [https://doi.org/10.1016/S0967-0637\(98\)00103-4](https://doi.org/10.1016/S0967-0637(98)00103-4)
- 1130 Smith, R. C., Martinson, D. G., Stammerjohn, S. E., Iannuzzi, R. A., & Ireson, K. (2008). Bellingshausen and western Antarctic Peninsula region: Pigment biomass and sea-ice spatial/temporal distributions and interannual variability. *Deep Sea Research Part II: Topical Studies in Oceanography*, 55(18), 1949–1963. <https://doi.org/10.1016/j.dsr2.2008.04.027>
- Spitz, Y. H., Moisan, J. R., & Abbott, M. R. (2001). Configuring an ecosystem model using data from the Bermuda Atlantic Time Series (BATS). *Deep Sea Research Part II: Topical Studies in Oceanography*, 48(8–9), 1733–1768.
- 1135 Stammerjohn, S. E., Martinson, D. G., Smith, R. C., Yuan, X., & Rind, D. (2008). Trends in Antarctic annual sea ice retreat and advance and their relation to El Niño–Southern Oscillation and Southern Annular Mode variability. *Journal of Geophysical Research: Oceans*, 113(C3). <https://doi.org/10.1029/2007JC004269>
- 1140 Steinberg, D. K., Ruck, K. E., Gleiber, M. R., Garzio, L. M., Cope, J. S., Bernard, K. S., Stammerjohn, S. E., Schofield, O. M. E., Quetin, L. B., & Ross, R. M. (2015). Long-term (1993–2013) changes in macrozooplankton off the Western Antarctic Peninsula. *Deep Sea Research Part I: Oceanographic Research Papers*, 101, 54–70. <https://doi.org/10.1016/j.dsr.2015.02.009>
- Stow, C. A., Jolliff, J., McGillicuddy, D. J., Doney, S. C., Allen, J. I., Friedrichs, M. A. M., Rose, K. A., & Wallhead, P. (2009). Skill assessment for coupled biological/physical models of marine systems. *Journal of Marine Systems*, 76(1), 4–15. <https://doi.org/10.1016/j.jmarsys.2008.03.011>
- 1145 Stukel, M. R., Asher, E., Couto, N., Schofield, O., Strelbel, S., Tortell, P., & Ducklow, H. W. (2015). The imbalance of new and export production in the western Antarctic Peninsula, a potentially “leaky” ecosystem. *Global Biogeochemical Cycles*, 29(9), 1400–1420. <https://doi.org/10.1002/2015GB005211>
- Taylor, K. E. (2001). Summarizing multiple aspects of model performance in a single diagram. *Journal of Geophysical Research: Atmospheres*, 106(D7), 7183–7192.
- 1150 Thibodeau, P. S., Steinberg, D. K., Stammerjohn, S. E., & Hauri, C. (2019). Environmental controls on pteropod biogeography along the Western Antarctic Peninsula. *Limnology and Oceanography*, 64(S1), S240–S256. <https://doi.org/10.1002/lno.11041>
- Tziperman, E., & Thacker, W. C. (1989). An Optimal-Control/Adjoint-Equations Approach to Studying the Oceanic General Circulation. *Journal of Physical Oceanography*, 19(10), 1471–1485.



- 1155 Vaughan, D. G. (2006). Recent Trends in Melting Conditions on the Antarctic Peninsula and Their Implications for Ice-sheet Mass Balance and Sea Level. *Arctic, Antarctic, and Alpine Research*, 38(1), 147–152. [https://doi.org/10.1657/1523-0430\(2006\)038\[0147:RTIMCO\]2.0.CO;2](https://doi.org/10.1657/1523-0430(2006)038[0147:RTIMCO]2.0.CO;2)
- Vaughan, D., Marshall, G., Connolley, W., Parkinson, C., Mulvaney, R., Hodgson, D., King, J., Pudsey, C., & Turner, J. (2003). Recent Rapid Regional Climate Warming on the Antarctic Peninsula. *Climatic Change*, 60, 243–274. <https://doi.org/10.1023/A:1026021217991>
- 1160 Ward, B. A., Friedrichs, M. A. M., Anderson, T. R., & Oschlies, A. (2010). Parameter optimisation techniques and the problem of underdetermination in marine biogeochemical models. *Journal of Marine Systems*, 81(1), 34–43.
- Weston, K., Jickells, T. D., Carson, D. S., Clarke, A., Meredith, M. P., Brandon, M. A., Wallace, M. I., Ussher, S. J., & Hendry, K. R. (2013). Primary production export flux in Marguerite Bay (Antarctic Peninsula): Linking upper water-column production to sediment trap flux. *Deep Sea Research Part I: Oceanographic Research Papers*, 75, 52–66. <https://doi.org/10.1016/j.dsr.2013.02.001>
- 1165 Whitehouse, M. J., Meredith, M. P., Rothery, P., Atkinson, A., Ward, P., & Korb, R. E. (2008). Rapid warming of the ocean around South Georgia, Southern Ocean, during the 20th century: Forcings, characteristics and implications for lower trophic levels. *Deep Sea Research Part I: Oceanographic Research Papers*, 55(10), 1218–1228. <https://doi.org/10.1016/j.dsr.2008.06.002>
- 1170